Faculty of Electrical Technology and Engineering

DESIGN AND DEVELOPMENT OF THE HIGHER ORDER FILTER UTILISING SYSTEMATIC DESIGN APPROACH FOR PWM BASED PV INVERTER

MUHAMMAD NABIL BIN ROSMAN

Bachelor of Electrical Engineering Technology (Industrial Power) with Honours

2023

DESIGN AND DEVELOPMENT OF THE HIGHER ORDER FILTER UTILISING SYSTEMATIC DESIGN APPROACH FOR PWM BASED PV INVERTER

MUHAMMAD NABIL BIN ROSMAN

A project report submitted
in partial fulfillment of the requirements for the degree of
Bachelor of Electrical Engineering Technology (Industrial Power) with Honours

Faculty of Electrical Technology and Engineering

UNIVERSITI TEKNIKAL MALAYSIA MELAKA

2023

UNIVERSITI TEKNIKAL MALAYSIA MELAKA
FAKULTI TEKNOLOGI KEJUTERAAN ELEKTRIK
BORANG PENGESAHAN STATUS LAPORAN
PROJEK SARJANA MUDA II

Tajuk Projek : Design and development of the higher order filter utilising systematic design approach for PWM based PV inverter

Sesi Pengajian : 2023/2024

Saya Muhammad Nabil bin Rosman mengaku membenarkan laporan Projek Sarjana Muda ini disimpan di Perpustakaan dengan syarat-syarat kegunaan seperti berikut:

1. Laporan adalah hakmilik Universiti Teknikal Malaysia Melaka.
2. Perpustakaan dibenarkan membuat salinan untuk tujuan pengajian sahaja.
3. Perpustakaan dibenarkan membuat salinan laporan ini sebagai bahan pertukaran antara institusi pengajian tinggi.
4. Sila tandakan (✓):

☐ **SULIT*** (Mengandungi maklumat yang berdarjah keselamatan atau kepentingan Malaysia seperti yang termaktub di dalam AKTA RAHSIA RASMI 1972)

☐ **TERHAD*** (Mengandungi maklumat terhad yang telah ditentukan oleh organisasi/badan di mana penyelidikan dijalankan)

☐ **TIDAK TERHAD**

Disahkan oleh:

(TANDATANGAN PENULIS)
Alamat Tetap: J8343 Taman Kesang Indah 5, 77000, Jasin, Melaka

(COP DAN TANDATANGAN PENYELIA)

Tarikh: 20 JANUARY 2024

Tarikh: 14 FEBRUARY 2024

*CATATAN: Jika laporan ini SULIT atau TERHAD, sila lampirkan surat daripada pihak berkuasa/organisasi berkenaan dengan menyatakan sekali tempoh laporan ini perlu dikelaskan sebagai SULIT atau TERHAD.

DECLARATION

I declare that this project report entitled "Project Title" is the result of my own research except as cited in the references. The project report has not been accepted for any degree and is not concurrently submitted in candidature of any other degree.

Signature	:	
Student Name	:	MUHAMMAD NABIL BIN ROSMAN
Date	:	20 JANUARY 2024

APPROVAL

I hereby declare that I have checked this project report and in my opinion, this project report is adequate in terms of scope and quality for the award of the degree of Bachelor of Electrical Engineering Technology (Industrial Power) with Honours.

Signature :

Supervisor Name : TS. MUHAMAD FAIZAL BIN YAAKUB

Date : 14 FEBRUARY 2024

DEDICATION

To my beloved mother, Aishah, and father, Rosman

ABSTRACT

In a distributed generation (DG) system, a higher-order filter plays an important role in improving the quality of the electrical power generated by the Photovoltaic (PV) system. However, the inherent resonance of high-order filters makes it difficult to manage the converter and to set the filter parameters. This project aims to design and develop a higher-order filter for a PWM based PV inverter using a systematic design approach. The project will involve designing the filter, constructing filter inductors and capacitor, testing and verifying the filter's performance in terms of THD and current ripple suppression. The expected outcome of the project is a higher-order filter design that will reduce high-frequency noise and harmonics, resulting in improved power quality and efficiency. The project's significance lies in its potential to advance power electronics research and improve the performance of PWM based PV inverters. In MATLAB, the LCL circuitry associated with H-bridge voltage source inverter was designed. In this thesis, a filter will be constructed by using parameters employed in simulations. The filters with different core permeabilities will be constructed and tested to compare how magnetic properties influence filter performance. The performance of the system was analysed using several kinds of observations. The results were compared and validated with theoritical value which this is certainly done by observing total harmonic distortion (THD) value below 5% in accordance to the IEEE 519- 1992.

ABSTRAK

Dalam sistem penjanaan teragih (DG), penapis peringkat lebih tinggi memainkan peranan penting dalam meningkatkan kualiti kuasa elektrik yang dijana oleh sistem fotovoltaik (PV). Walau bagaimanapun, resonans yang hadir pada penapis peringkat lebih tinggi akan menyukarkan pengurusan dalam penukar dan untuk menetapkan parameter penapis. Projek ini bertujuan untuk membentuk dan membangunkan penapis peringkat lebih tinggi untuk penyongsangan PV berasaskan PWM dengan menggunakan pendekatan reka bentuk yang sistematik. Projek ini akan terlibat dengan pembentuk penapis, membina induktor dan kapasitor penapis, menguji dan mengenal pasti prestasi penapis dari segi THD dan penghapusan talian arus. Hasil yang dijangkakan daripada projek ini ialah reka bentuk penapis peringkat lebih tinggi yang akan mengurangkan frekuensi yang tinggi dari segi gangguan luar dan harmonik, menghasilkan kualiti dan kecekapan kuasa yang lebih baik. Kepentingan projek ini terletak pada potensi untuk memajukan penyelidikan elektronik kuasa dan meningkatkan prestasi penyongsangan PV berasaskan PWM. Di dalam MATLAB, litar LCL yang dikaitkan dengan penyongsangan sumber voltan H-bridge telah direka bentuk. Prestasi sistem dianalisis menggunakan beberapa jenis parameter. Dalam tesis ini, satu penapisakan dibina dengan menggunakan parameter yang digunakan dalam simulasi. Penuras dengan perbezaan kebolehtelapan teras yang berbeza akan diuji untuk membandingkan bagaimana sifat magnetik mempengaruhi prestasi penapis. Prestasi sistem dianalisis menggunakan beberapa jenis pemerhatian. Keputusan simulasi ini kemudian dibandingkan dan disahkan dengan nilai teori yang dilakukan dengan mmerhatikan jumlah herotan harmonik (THD) di bawah 5% mengikut standard IEEE 519-1992.

ACKNOWLEDGEMENTS

First and foremost, I would like to express my gratitude to my supervisor, Ts. Muhammad Faizal bin Yaakub for their precious guidance, words of wisdom and patient throughout this project.

I am also indebted to Universiti Teknikal Malaysia Melaka (UTeM) for the support which enables me to accomplish the project. Not forgetting my fellow colleague for the willingness of sharing his thoughts and ideas regarding the project.

My highest appreciation goes to my parents, and family members for their love and prayer during the period of my study. An honourable mention also goes to my friends for all the motivation and understanding.

Finally, I would like to thank all the staffs at the Faculty of Electrical Technology and Engineering, fellow colleagues and classmates, the Faculty members, as well as other individuals who are not listed here for being co-operative and helpful.

TABLE OF CONTENTS

LIST OF TABLES

LIST OF FIGURES

LIST OF SYMBOLS

f_g	-	Grid frequency or fundamental frequency in Hertz
f_{sw}	-	PWM carrier frequency
ω_{res}	-	Resonance frequency
P_n	-	Rated active power
E_n	-	Line to line RMS voltage
V_{DC}	-	DC link voltage
L_1	-	Inverter side inductor
L_2	-	Grid side inductor
C	-	Capacitor
R_d	-	Damping Resistor
V_g	-	Grid Voltage
ω_o	-	Grid Angular Frequency
V_i	-	Input DC Voltage
r	-	Ratio
V_{AN}	-	Inverter Terminal Voltage
V_{BN}	-	Inverter Terminal Voltage
Vcr	-	Carrier Signal
Vm	-	Reference Signal

LIST OF ABBREVIATIONS

DG	-	Distributed Generation
PV	-	Photovoltaic
PWM	-	Pulse – Witdh Modulation
DC	-	Direct Current
AC	-	Alternative Current
THD	-	Total Harmonic Distortion
SPWM	-	Sinusoidal Pulse – Witdh Modulation
VSI	-	Voltage Source Inverter
VAR	-	Voltage – Ampere Reactive

CHAPTER 1

INTRODUCTION

1.1 Background

In recent years, renewable energy sources are utilized to fulfill the energy requirements of residential, commercial, and industrial sectors due to the rapid increase in electricity demand. Many technologies of power conversion devices have been developed for applications such as photovoltaic (PV) inverters which makes it extremely important. PV inverters play a important role in the conversion process of direct current (DC) power produced by solar panels into alternating current (AC) power. This conversion enables the AC power to be either fed into the electrical grid or consumed locally for residential, commercial, or industrial purposes. The inverters used Pulse-Width Modulation PWM techniques to achieve efficient power conversion and control. One of the critical component in a PV inverter is the higher-order filter, which is responsible for filtering out harmonics and ensuring high-quality power output. Interconnecting an inverter to the utility grid often involves the used of a low-pass filter. The low-pass filter is an important component which helps prevent the introduction of harmonics caused by the use of Pulse-Width Modulation (PWM) switching technique [1]. Thus, these filters offer several advantages, including high attenuation capabilities, improved performance, cost-effectiveness, and reduced weight and size.

1.2 Problem statement

Solar photovoltaic (PV) systems have gained significant attention as a clean and renewable energy source. To convert the DC power generated by PV panels into AC power for grid integration or local consumption, power electronic inverters are employed. Pulse Width Modulation (PWM) switching techniques are commonly used in PV inverters for efficient power conversion and control [2]. However, PWM operation can introduce unwanted harmonics and high-frequency switching noise into the output voltage waveform, which may affect the performance and reliability of the PV system. It is also the main factor causing problems to sensitive equipment. In order to prevent undesired high-frequency signals from entering the distribution system, the switching technique needs the application of a low-pass filter. In the output stage of the converter, various types of low-pass filters such as L, LC, LCL, or other higher order filters are employed to mitigate high-frequency noise and harmonics. These filters effectively attenuate undesired frequencies, ensuring a cleaner and smoother output waveform. Among them, LCL is a filter that shows a significant reduction in high-frequency noise, harmonic and improves switching ripple reduction effectively compared to the other filters. Although LCL filters offer numerous advantages, their design process can be complex, requiring careful consideration to optimize their performance. Thus, a well defined design process is required to enhance the performance of the filters. Hence, in this study, several parameters have to be reconsidered to reduce things that can cause instability to the system.

1.3 Project Objective

The main aim of this project is to design and develop a higher-order filter using a systematic design approach for a PWM-based PV inverter. The project aims to achieve the following goals:

a) To design a higher-order filter using a systematic design approach procedure that meets the filter's specifications, such as cutoff frequency and order.

b) To construct filter inductors using various ferrite core types permeability.

c) To test and verify the performance of the designed filter in terms of THD (total harmonic distortion) and current ripple suppression.

1.4 Scope and limitations of Project

The scope of this study will consider specific values for the DC-Link Voltage and Grid frequency, set at 110 Vrms and 60 Hz, respectively. The primary focus will be on designing and implementing an LCL filter, with particular attention given to utilizing resonant control as the controller. This approach aims to enhance performance and stability of the filter. The study will leverage Matlab/Simulink for the design and simulation of the LCL filter, utilizing the software's capabilities to model the filter's behavior and evaluate its performance. Additionally, the study will explore the application of Matlab simulation software, specifically the Continuous Block within Simulink, to gain insights into its utilization for modeling filter.The ideal values for the inductor and capacitor in the LCL filter will be derived through calculations to optimize performance. Lastly, the study will analyze and apply the guidelines and requirements outlined in the IEEE 519-1992 standard for harmonic control, ensuring compliance and addressing harmonic issues in the LCL filter design.

1.5 Overview of project

This thesis has a total of five chapters, begin with the background on the use of filters in PV inverters, followed by a problem statement, objectives, and scope of study.

Second chapter or Chapter 2 discusses on the chosen literature review of the studies which come from different resources. All of the resources used in this study came from earlier research that was related and could be implemented to fulfill the objectives of this study.

Next in Chapter 3, methodology of this study discusses the flow and software involved throughout completing the project. To illustrate the process and flow of this study, flowcharts are used so that a better understanding can be gained. Besides that, this chapter explains the procedures of simulation analysis, including the parameters and components used.

In Chapter 4, the results of the filtered and unfiltered pulsed waveforms will be compared and discussed. This chapter also includes the validation of simulation results.

Last chapter which is Chapter 5 explains about the conclusion of this study and also briefly summarize the filter results that have been designed

CHAPTER 2

LITERATURE REVIEW

2.1 Introduction

Power electronic systems rely heavily on low-pass filters because they are capable of minimizing problems including current harmonics, voltage distortion, and system instability. In order to analyse higher-order filters, it is very important to refer the previous research escpecially theory and fundamentals of the study depending on method and parameter used in the filter.

2.2 Classification PV Systems

The PV system can be connected to either a low voltage or medium voltage system. The classification of grid connected PV systems' topology is a crucial aspect of their design. The number of power conversion stages determines whether the system is a single stage or dual stage system [3]. This classification has been widely adopted in the literature to describe the different topologies of grid-connected PV systems [3]. Figure 2.1 below shows a single while Figure 2.2 below shows a dual stage PV systems.

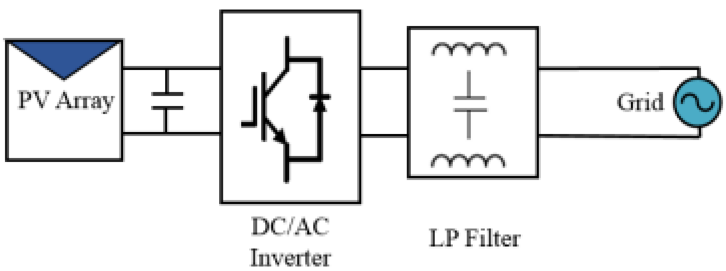

Figure 2.1 : Single stage PV systems (Hamza O Khalfalla, 2019)

In a single-stage configuration, the grid-connected PV system has only one power inverter that responsible for converting DC energy into AC components [3]. This inverter is expected to handle all tasks, such as implementing a maximum power point tracking (MPPT) algorithm to optimize power extraction from PV panels, regulating the output current, and ensuring synchronization with the grid [4]. Since it only has one power conversion device, single stage PV system provides many advantages such as simple topology, high efficiency, high power density, and lower cost [5].

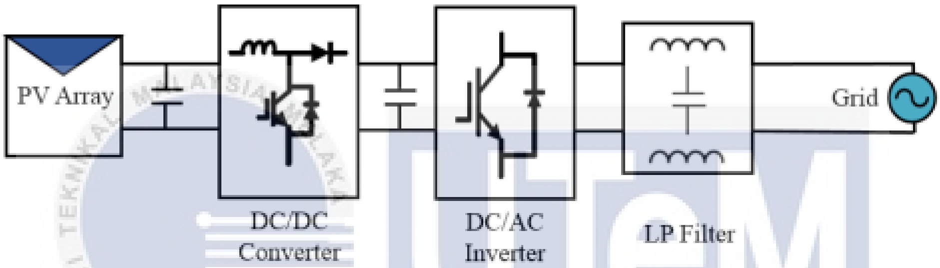

Figure 2.2 : Dual stage PV systems (Hamza O Khalfalla, 2019)

Dual stage PV systems as shown in Figure 2.2 is the most common approach in grid connected PV inverter systems. In the initial stage of their system, a boost or buck-boost type DC/DC converter is the most frequently used [3]. This additional converter is installed between the PV arrays and the inverter. The maximum power point tracking (MPPT) control approach will be used for the DC/DC power conversion, which has the advantage of controlling and extracting the maximum power from the solar panel [6]. The second stage of the system is the DC/AC inverter, which controls the output current of the inverter. Thus, when comparing these two topologies, the second stage system is capable of operating with a larger power capacity compare to single stage system [3].

So, related to this study, the low pass filter is an important component in the system and it is located at the inverter output. The filter's function is to prevent harmonic components generated by the high PWM switching frequency from being introduced into the grid. Thus, L, LC, and LCL filters are the three most often used filter types.

2.3 PWM Based PV Inverter

Figure 2.3 below shows a H-bridge inverter circuit using four metal-oxide-semiconductor field-effect transistor (MOSFET). Inverters are devices that take a DC voltage source and a DC current source to turn it into an AC voltage and current [2]. The input to the PV inverter is a DC source. Using a power conversion stage, the DC power generated by the solar panels is first converted to a high-frequency AC voltage. The PV inverter is typically operated using a switching technique known as pulse-width modulation (PWM). In power electronics, there are two switching technique that are often used which is bipolar PWM and unipolar PWM [3]. However, PWM switching technique will generates harmonics and causes the system unstable. Thus, a low-pass filter is needed to make sure that the unwanted high-frequency signals don't get through the distribution system. Furthermore, according to IEEE Standard 519-1992, the total harmonic distortion (THD) of an inverter's output current should be below 5% [7].

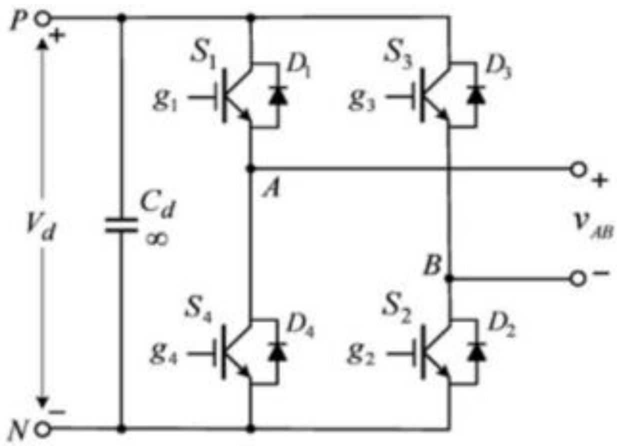

Figure 2.3 : H-bridge inverter using four MOSFET (Namboodiri, A.V., & Wani, H.S. 2014)

2.3.1 Bipolar PWM

Bipolar PWM works by comparing two waveforms to produce a control signal. The waveform compared is a single sine waveform (reference signal), v_m with a rectangular waveform (carrier signal), v_{cr} as shown in Figure 2.4 and Table 2.1 [3]. In this scheme, the transistors (S_1,S_2) and (S_3,S_4) are turned ON and OFF according to the control signal [8]. Therefore, it is necessary to consider only two independent gating signals v_{g1}, v_{g3} generated by the comparison between v_m and v_{cr} . The inverter terminal voltage is identified as V_{AN} and V_{BN}, so the inverter output voltage can be found through Equation 2.1 [8].

$$V_{AB} = V_{AN} - V_{BN} \tag{2.1}$$

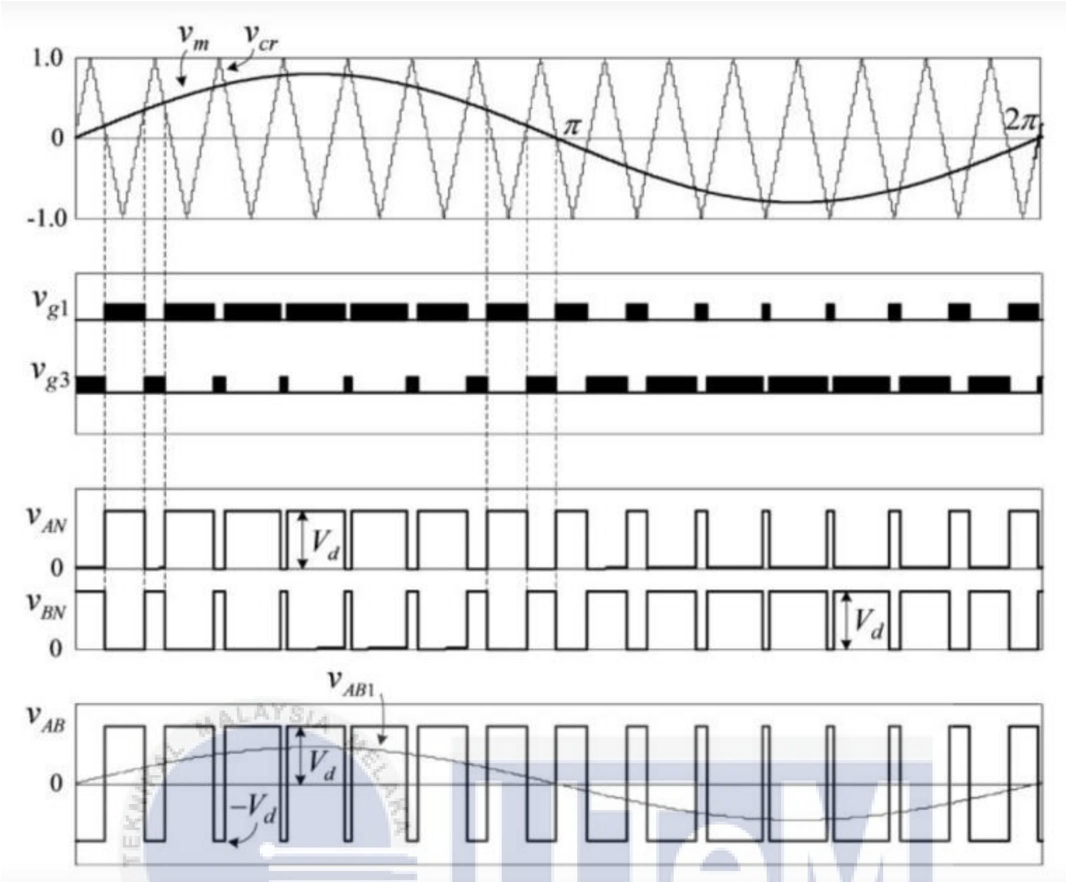

Figure 2.4 : Waveform for Bipolar PWM switching (Namboodiri, A.V., & Wani, H.S. 2014)

Table 2.1 Comparison of v_m and v_{cr} for Unipolar PWM

Signals Comparison	**S_1**	**S_2**	**S_3**	**S_4**
$v_m > v_{cr}$	ON	ON	OFF	OFF
$v_m < v_{cr}$	OFF	OFF	ON	ON

2.3.2 Unipolar PWM

Unipolar PWM also works by comparing two waveforms to produce a control signal but it shifted from each other by 180° as shown in Figure 2.5 and Table 2.2 [3]. Transistor (S_1,S_3) will not switch ON simultaneously with transistors (S_2,S_4). This scheme shows the difference with Bipolar PWM where all four transistors are switched at the same time [8]. Therefore, it is necessary to consider only two independent gating signals v_{g1}, v_{g3}

generated by the comparison between v_m and v_{cr} for transistor (S_1, S_3). Inverter output voltage will switch between zero and $+V_d$ during positive cycle or between zero and $-V_d$ during negative cycle [8]. Thus, unipolar PWM corresponding voltage can be described based on the switching state as Table 2.2 .

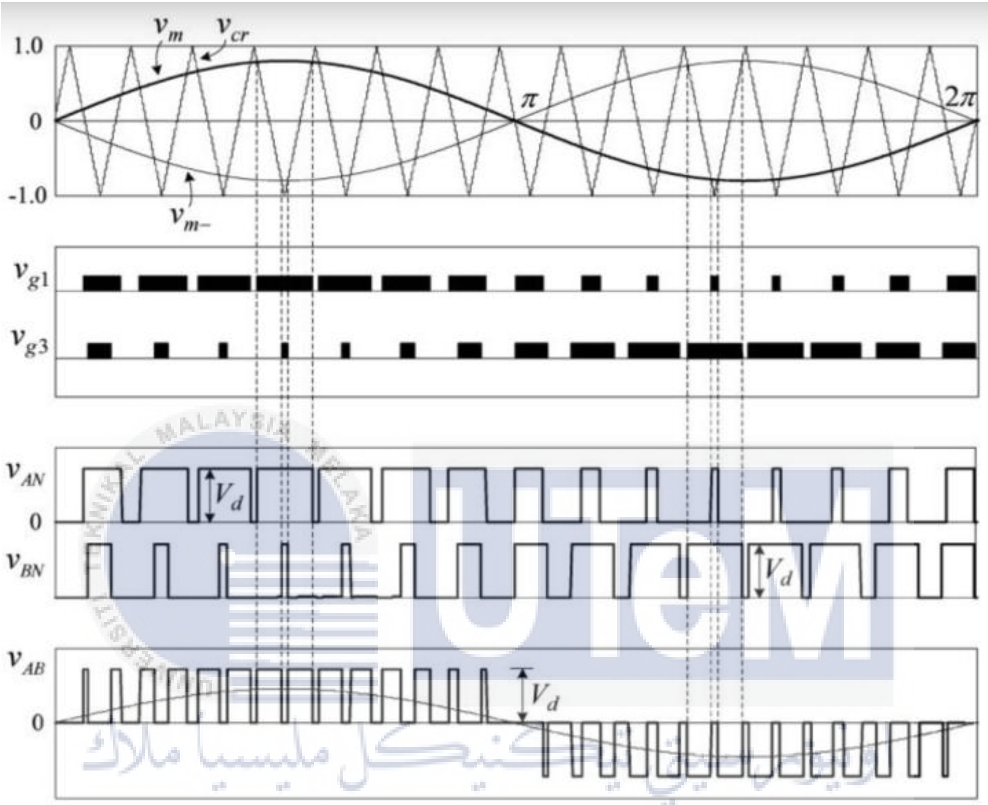

Figure 2.5 : Waveform for Unipolar PWM switching (Namboodiri, A.V., & Wani, H.S. 2014)

Table 2.2 : Unipolar PWM corresponding voltage

S_1	S_2	S_3	S_4	V_{AN}	V_{BN}	V_{AB}
ON	OFF	OFF	ON	V_d	0	V_d
OFF	ON	ON	OFF	0	V_d	$- V_d$
ON	OFF	OFF	ON	V_d	V_d	0
OFF	ON	ON	OFF	0	0	0

2.4 Total Harmonic Distortion (THD)

Based on the search, Total Harmonic Distortion (THD) is the main problem in the power system because it affects the power quality [9]. One of the methods to reduce total harmonic distortion THD is by adding a Passive filter which will be discussed next. Harmonic distortion is measured by applying a spectrally pure sine wave to the filter and observing the output spectrum [10]. The amount of harmonic distortion present at the filter output is determined by the following factors [10] :

- Frequency response of the filter.
- Load applied to the output of filter.
- Filter's power supply voltage.
- Internal inductor's impedance and Q factor.
- Number of inductor element presence.
- Circuit board layout.
- Grounding.
- Thermal management.

Harmonic content as shown in Figure 2.6 Below is an example of output harmonic spectrums that will be analyzed and expressed by using Equation 2.2 and Equation 2.3 [10].

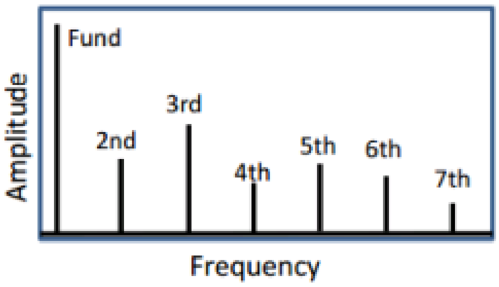

Figure 2.6 : Common harmonic content (M. Safwan b. M. Masarik, 2017)

If the obtained measurement data is in power, then

$$\text{THD (\%)} = \sqrt{\frac{P_1+P_2+P_3+\ldots+P_n}{P_1}} \times 100 \tag{2.2}$$

Where P_n must in Watts

If the obtained measurement data is in voltage, then

$$\text{THD (\%)} = \sqrt{\frac{V_1+V_2+V_3+\ldots+V_n}{V_1}} \times 100 \tag{2.3}$$

Where V_n must in RMS Voltage

2.4.1 THD Reduction using Passive Filters

The usage of passive filters is a commonly used technique for reducing THD in various systems including the PV systems. Figure 2.7 shows Single Phase Representation of Nonlinear Load and Passive Shunt Filter. Passive filters are widely used for mitigating harmonics in power systems because of the increasing of non-linear loads in power systems. The ease of installation and low pricing are the device's greatest advantages. However, large different filter sizes may be required for various harmonic orders, which could be very costly [11]. Also, several filters may have an effect on system stability since they can bring the entire system into the resonance area. If more inductors or capacitors are used, the circuit might become bulky [12]. A passive filter has the ability to eliminate targeted harmonics which is the 3rd harmonic [13]. It should be noted that the resonance frequency needs to be lower than the fundamental harmonic frequency to avoid shift from the filter caused by parameter changes in the filter [13].

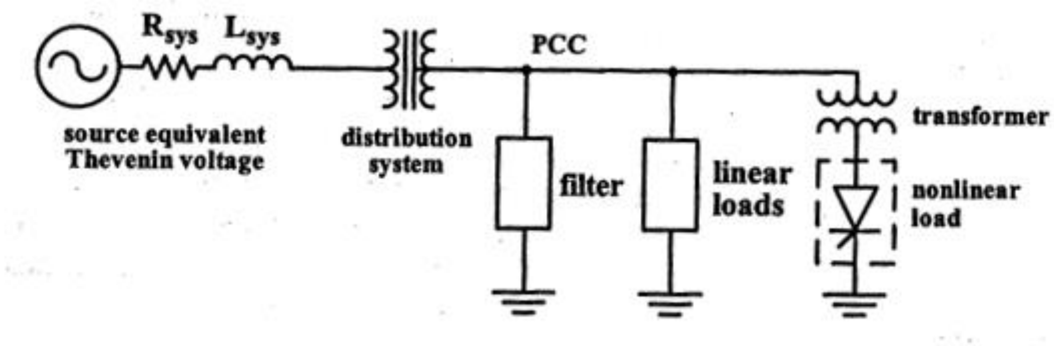

Figure 2.7 : Single Phase Representation of Nonlinear Load and Passive Shunt Filter (Liqaa Alhafadhi, 2016)

2.5 Filter Topologies

The switching of semiconductor devices causes harmonics in the generated current, which can be reduced by using the output filter . There are various types of filters. The filter which consist of inductor connected to the output of the inverter is the simplest one. However, different ways of connecting inductors and capacitors, such as LC or LCL can be applied [14]. Thus, Figure 2.8 shows the schematic diagram of a single phase grid-connected inverter with an LCL filter.

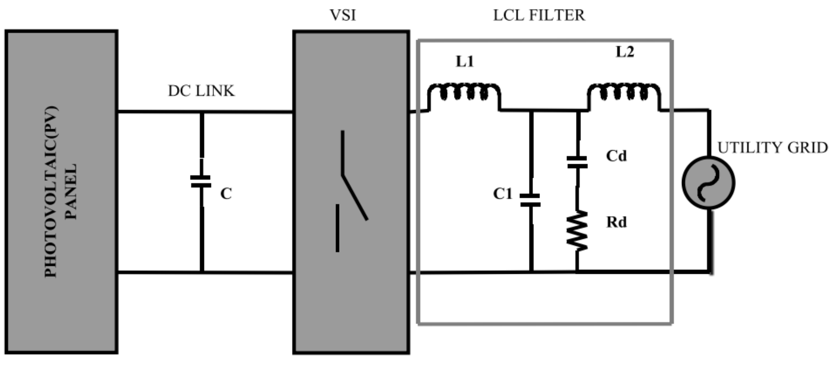

Figure 2.8 :Single Phase Grid Connected Inverter along with LCL Filter (Liqaa Alhafadhi, 2016)

2.5.1 L Filter

The L filter was one of the most famous filter until the IEEE 519- 1992 standards were released [15]. L filter are commonly used to suppress noise and unwanted signals in electronic circuits. They can attenuate high-frequency noise while allowing low-frequency signals to pass through. In order to meet all of the standards' requirements, the L filter grade and size have to be very high [14]. For all frequencies, the L-Filter's attenuation is 20 dB per decade, making it a first-order filter. Since the attenuation is suitable for high-frequency switching converters, they are a good choice. In contrast, inductance drastically decreases the filter dynamics of the entire system converter [14].

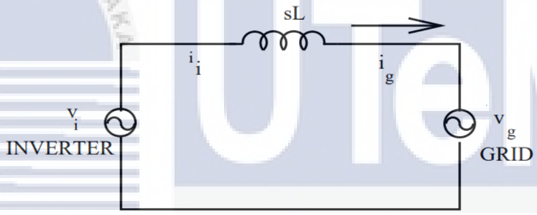

Figure 2.9 : L filter positioned between active front end and grid (Deepika Kumari 2014)

Based on previous work, an analysis was carried out to identify the reliability of the Photovoltaic (PV) system [15]. It has been shown that the Total Harmonic Distortion (THD) produced by L filter is high compare to Total Harmonic Distortion produced by LCL filter with the same active power injection as shown in the Table 2.3 [15]. Therefore, the use of the L filter in the PV system is not recommended because the amount of THD produced is high and does not meet the objectives of this study.

Table 2.3 : THD produced from L and LCL filter

	L_1	C	L_2	THD
L Filter	2.56mH			0.382%
LCL Filter	425 µH	9.9 µH	85 µH	0.00926%

2.5.2 LC Filter

When compared to the L filter, the LC-Filter is a second-order filter with greater damping characteristics [14]. The design of the filter is user-friendly and efficient with fewer problems during usage. LC filters are used in audio applications for signal filtering and equalization. They can help shape the frequency response and remove unwanted frequencies or noise from audio signals. This filter has no gain before the cut-off frequency f_o, but it has a peaking effect at the resonant frequency, f_o [14]. The amount of attenuation provided by this filter is 12 dB per decade after the cut-off frequency, f_o. Thus, a damping circuit is introduced to the filter to supress the undesirable behaviour near the cutoff frequency. In additional, the damping may be either parallel or in series [16]. Transfer function for LC-Filter is as Equation 2.4 [14].

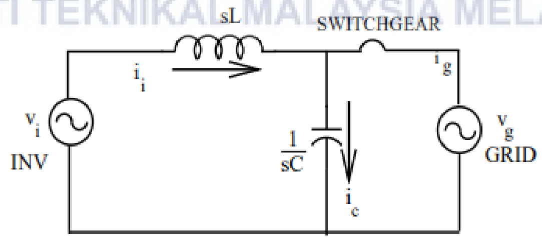

Figure 2.10 :LC filter positioned between active front end and grid (Parikshith B.C, 2009)

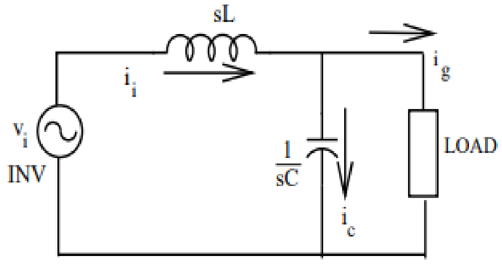

Figure 2.11 :LC filter positioned between active front end and stand-alone load (Parikshith B.C, 2009)

$$F(s) = \frac{1}{1+ L_F + s^2 L_F C_F} \tag{2.4}$$

Where

L_F = Filter Inductor

C_F = Filter Capacitor

Based on previous work, an analysis was carried out to compare the effect of LC filter for Photovoltaic (PV) system [17]. The study has compared the Total Harmonic Distortion (THD) produced when the system is simulated with and without a filter. It shows that the use of LC filter provides a lot of involvement to reduce harmonics in the system as can be seen in the Figure 2.12 and Figure 2.13. Table 2.4 summarizes the comparison of THD present in the system. Thus, it proves that LC-Filter is one of the suitable filters to reduce harmonics in PV system.

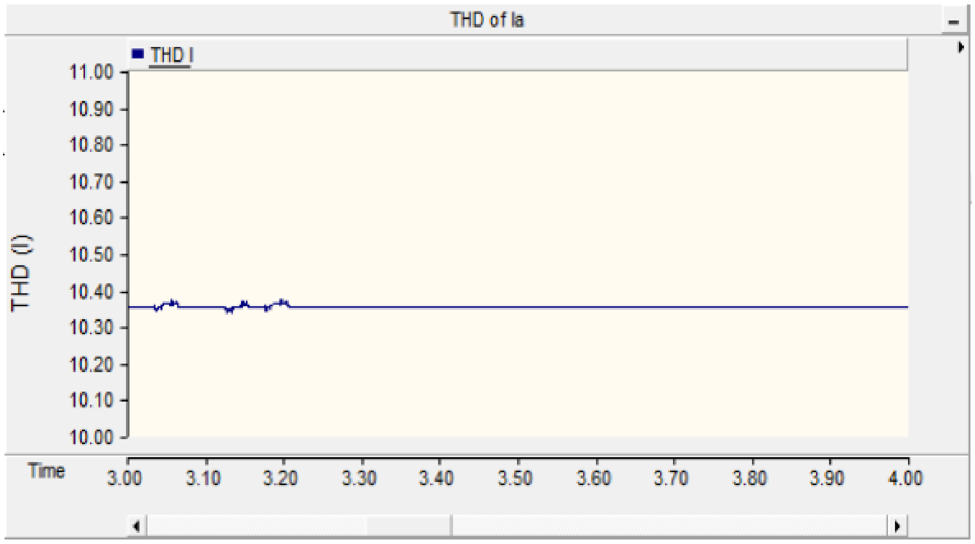

Figure 2.12 : Total Harmonic Distortion without filter (Parikshith B.C, 2009)

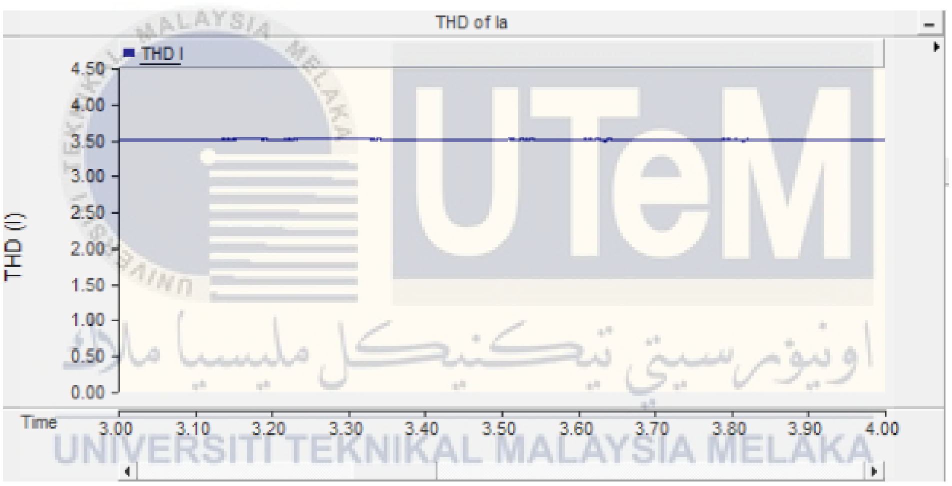

Figure 2.13 : Total Harmonic Distortion with LC filter (Parikshith B.C, 2009)

Table 2.4: THD results in PV system without filter and with LC filter

THD	**THD_V (%)**	**THD_I (%)**
Without filter	10.35	10.35
LC filter	3.5	3.5

2.5.3 LCL Filter

The LCL filter is a third-order filter that exhibits a attenuation rate of 60dB per decade for frequencies beyond the resonance frequency [14]. This means that a lower switching frequency could be used for the converter switches. LCL filters are extensively used in grid-connected inverters to mitigate harmonics and improve power quality when injecting power into the utility grid. Based on the findings, it is better to decoupling the filter from the grid-connected inverter with grid side impedance [14]. As a result, the current ripple experienced by the grid inductor may be reduced. Additionally, the LCL filter will be susceptible to oscillations and amplify frequencies close to its cut off frequency. Therefore, damping is added into the filter to mitigate the impact of resonance [16]. The equivalent circuit for LCL filter can be described at Figure 2.14.

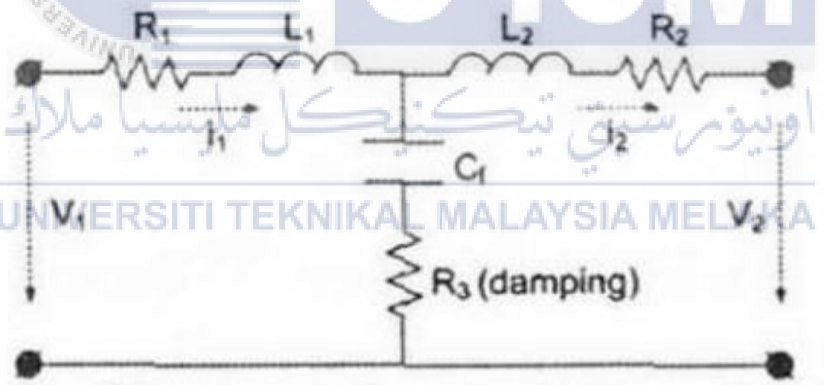

Figure 2.14 : LCL Filter equivalent circuit diagram (Cha H., Vu T. K. 2009).

R1 and R2 will be ignored due to their small resistance values [18]. Therefore, the transfer function for the LCL filter from input V1 to output i2 can be described as follows:

$$G(s) = \frac{i_2(s)}{V_1(s)} = \frac{C_f R_3 s + 1}{L_1 L_2 C_f s^3 + (L_1 + L_2) C_f R_3 s^2 + (L_1 + L_2) s} \tag{2.5}$$

Where

V_1 = Inverter output voltage

i_2 = Output current

L_1 = Filter Inductor

L_2 = Grid side Inductor

C_f = Filter Capacitor

R_3 = Damping resistor

Based on previous work, an analysis was carried out to design LCL Filter for grid connected inverter application [19]. The study has compared the current and voltage ouput when the system is simulated with and without a filter as ashown in Figure 2.15. In addition, the study also compared the Total Harmonic Distortion (THD) by using the FFT analysis in the inverter side inductor with the grid side inductor as shown in Figure 2.16 and Figure 2.17. Both of these analyzes give a good results where the harmonics produced during DC/AC power conversion have been reduced. Meanwhile, the THD obtained also shows a very good reduction and it meets the IEEE 519-1992 standard. Thus, LCL filter is fits for this application.

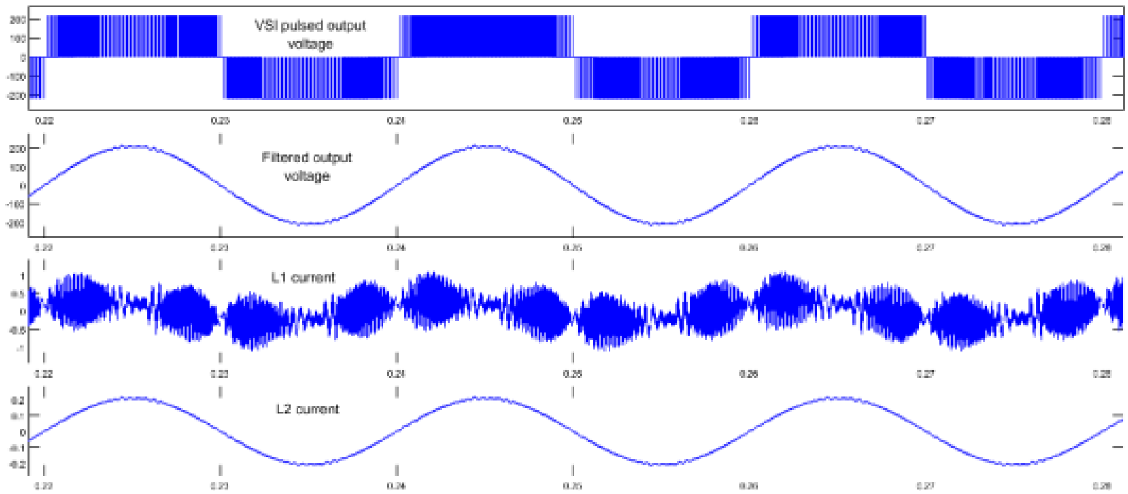

Figure 2.15 : Output current and voltage waveform (Yaakub, M. F., Radzi, M. A. M., Asri, M., Shafie, S., Azis, N., & Noh, F. H. M., 2021)

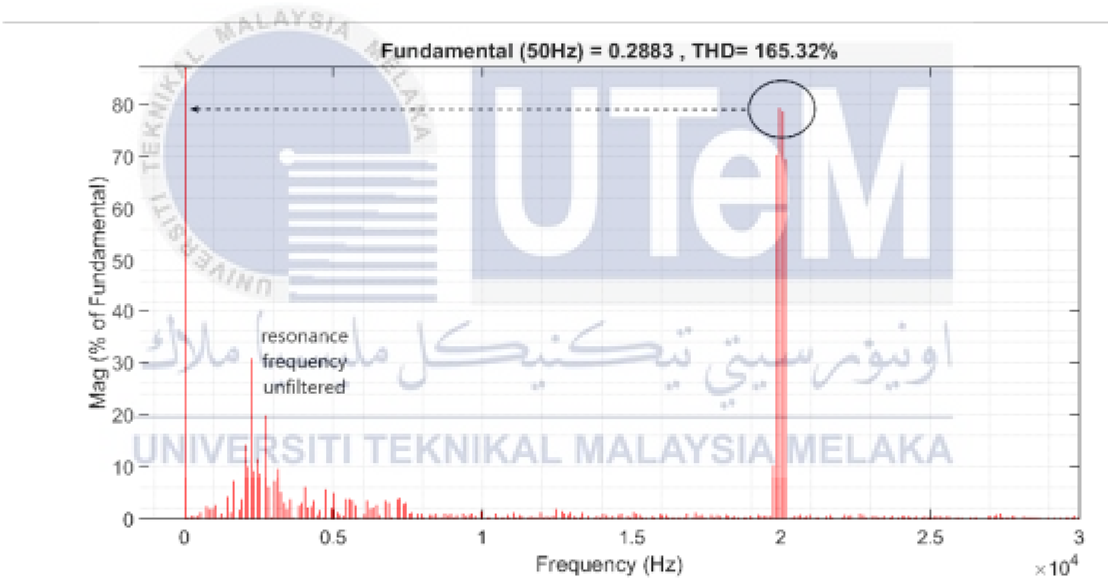

Figure 2.16 : FFT analysis of the current at inverter side filter (Yaakub, M. F., Radzi, M. A. M., Asri, M., Shafie, S., Azis, N., & Noh, F. H. M., 2021)

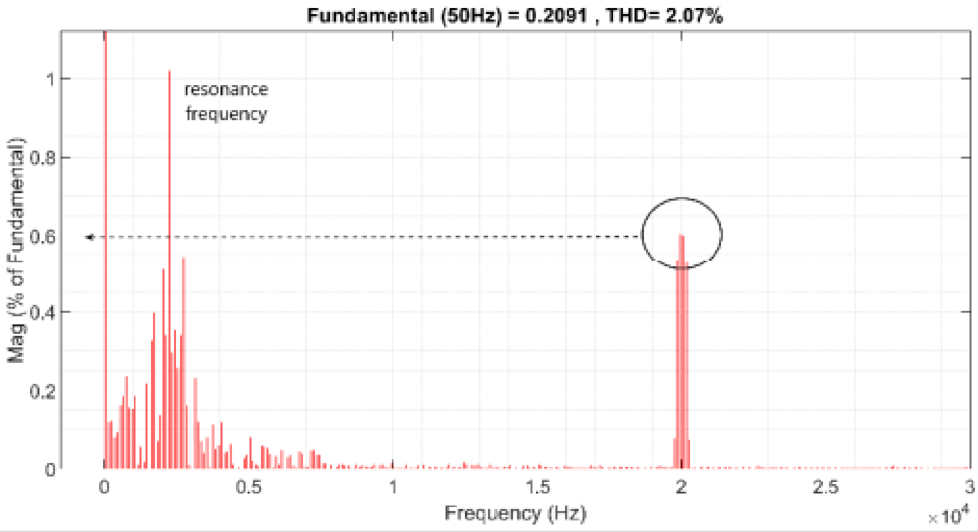

Figure 2.17 : FFT analysis of the current at grid side filter (Yaakub, M. F., Radzi, M. A. M., Asri, M., Shafie, S., Azis, N., & Noh, F. H. M., 2021)

2.6 LCL Filter Design Considerations

A simple first order L filter is not only bulky but also fails to satisfy the standard harmonic attenuation specifications [20]. Currently, a third order LCL filter is commonly used to attain higher attenuation and standards while reducing the size and cost of the components. However, the process design of an LCL filter is difficult. To realise a basic LCL-filter design method, it considers the relationships listed below [21] :

- Attenuation of current ripple,
- Resonance frequency
- Ratio between grid-side and inverter-side inductors
- Damping resistor

2.6.1 Attenuation of Current Ripple

So, usually, the high-frequency current ripple attenuation of the filter is affected by the LC part [22]. So, it is very important to understand the influence of inductance because it plays a significant role in controlling current ripple in the system. A larger ripple current causes the system to produce more noise and distortion. Therefore, a proper inductor design is required to reduce the current ripple. So based on previous work that has been done, it can be overcome by increasing the switching frequency, f_{sw} [22]. Figure 2.18 has shown how current ripple can be reduced by having a larger modulation index .

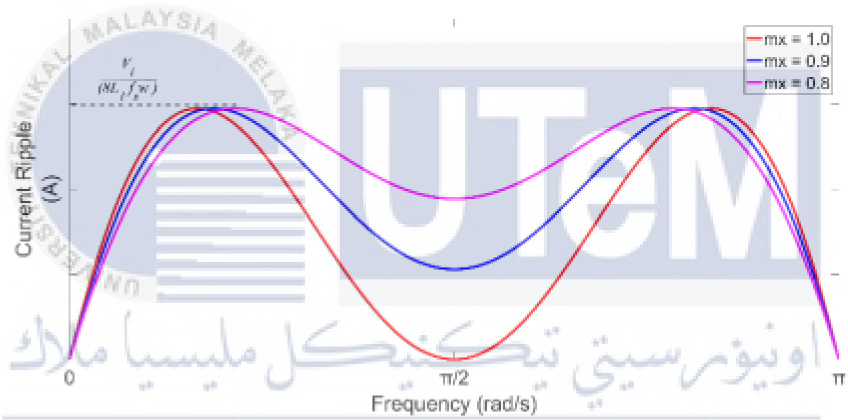

Figure 2.18 : Current ripple magnitude distribution (Yaakub, M. F., Radzi, M. A. M., Azri, M., & Noh, F. H. M., 2021)

Therefore, by assuming unipolar sinusoidal pulse width modulation (SPWM) with a unity power factor, the maximum current ripple, I_{rpmax} at the filter output is as follows [19]:

$$I_{rpmax} = \boldsymbol{\beta}_c I_1 = \frac{V_i}{8L_1 f_{sw}} \tag{2.6}$$

Where,

Vi = input DC voltage

L_1 = inverter side inductance

f_{sw} = switching frequency

The allowable current ripple coefficient $\boldsymbol{\beta}_c$ is usually 5% to 30% of the rated current, depends on system usage [19] .Note that coil size and core losses inversely affect this value. By lowering the ripple value, it will also reduces the system's switching and conducting losses[19].

2.6.2 Resonance frequency

The LCL filter will cause resonance frequency issues, making the design process more challenging [23]. The resonance frequency determines the frequency at which the filter exhibits the highest impedance, and it plays a crucial role in the filter's performance and stability[23]. This must be avoided in the PWM and filter design. The grid inductance variation occurs because the filter is able to absorb any changes that occur in the grid inductance value [24]. So, based on the previous work, grid inductance variation will change the resonance frequency [24]. By considering the change in grid inductance, the resonance frequency, ω_{res} can be calculated by using equation 2.7.

$$\omega_{res} = \sqrt{\frac{L_1+L_2+L_g}{L_1(L_{2+}L_g)C_f}} \tag{2.7}$$

Where,

L_1 = Filter Inductor

L_2 = Grid side Inductor

L_g = Grid Inductance

C_f = Filter Capacitor

The resonance frequency, ω_{res}, is proportional to the inductance ratio, r which depends on the position of the voltage and current sensors on the filter [24]. Based on the previous work, ratio, r = 1 will result in the lowest possible inductance and capacitance, resulting in the best possible performance in terms of voltage drop, switching losses, dynamic response, reactive power, energy storage in the LCL-filter, attenuation of switching harmonics, cost, and grid impedance variation [25]. Therefore, the resonance frequency, ω_{res} also can be calculated by using equation 2.8.

$$\omega_{res} = \frac{Z_B}{L_1}\sqrt{\frac{1+r}{r}} \tag{2.8}$$

Where,

L_1 = Filter Inductor

Z_B = Base Impedance

r = Inductance ratio

The angular resonance frequency, ω_{res} is then simplified further by taking into account the stiff grid condition as shown in Equation 2.9 [24]. And finally, with the existence of the filter capacitor, C_f, grid-side inductance, L_2 is defined with respect to the inductance ratio, r as in Equation 2.10.

$$\omega_{res} = \sqrt{\frac{L_T}{L_1 L_2 C_F}} \tag{2.9}$$

Where, $L_T = L_1 + L_2$.

$$L_2 = rL_1 \tag{2.10}$$

Based on finding, Equation (2.8) can be proved by finding the relationship between between resonance frequency, ω_{res} and inductance ratio, r [24]. Therefore, Figure 2.19 shows that increasing the resonance frequency will also increase the value of inductance ratio.

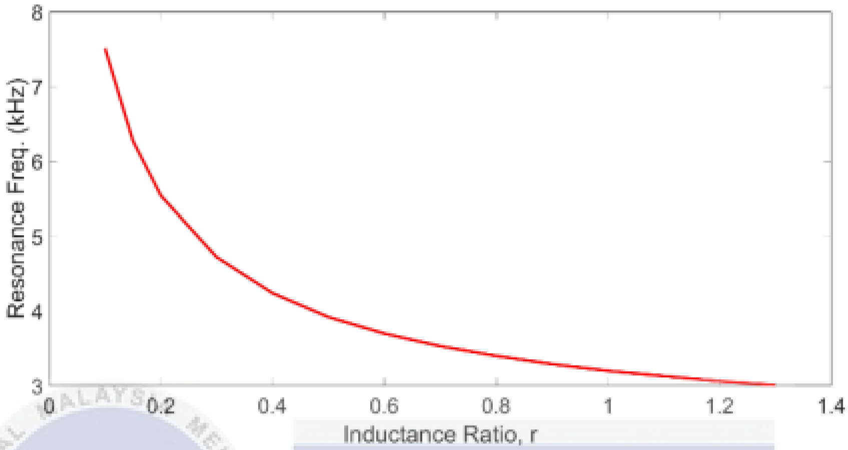

Figure 2.19 : Relationship between resonance frequency, ω_{res} and inductance ratio, r (Yaakub, M. F., Radzi, M. A. M., Azri, M., & Noh, F. H. M., 2021)

2.6.3 Damping

Due to the addition of zeros and poles, the LCL filter will produce a resonance frequency, making the entire system unstable [26]. Therefore, the system needs proper damping to avoid attenuation problems that will interfere with the effectiveness of the LCL filter. It is crucial to pay attention to the resonance frequency, ω_{res} of the filter to prevent higher current ripple.

2.6.3.1 Passive Damping

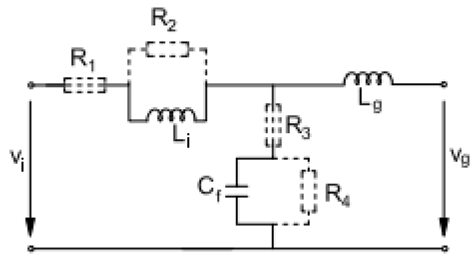

Figure 2.20 : Passive damping circuit with the damping possible positions, R. Pena-Alzola, M. Liserre, F. Blaabjerg, M. Ordonez, and Y. Yang, (2014)

Passive damping can be achieved by introducing resistance into the filter circuit, which is commonly accomplished with series or parallel resistors. There are four possible positions to place the damping as shown in Figure 2.20. A passive damping, has been chosen for LCL filter designing, and the implementation involves placing a resistor in series with the capacitance of the filter [19]. This approach is extensively used since it is simple and easy to implement. Basically, Equation (2.11) involving the capacitance of the filter used to determine the damping resistor for the filters. Specifically when the damping resistor value is equal to one-third of the filter capacitor's impedance [19].

$$R_d = \frac{1}{3\omega_{res}C_f} \tag{2.11}$$

Higher damping resistor value in the LCL filter will make the system become more stable as illustrated in Figure 2. [24]. However, it also results in higher losses due to increased power dissipation across the resistor. Thus, a damping resistor with an appropriate value provides is needed to prevent losses in the system .

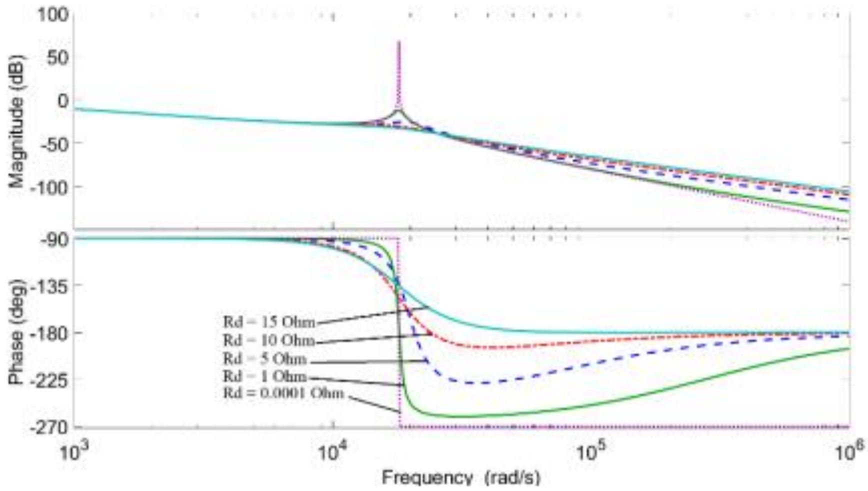

Figure 2.21 : Effect of various damping values on system stability (Yaakub, M. F., Radzi, M. A. M., Azri, M., & Noh, F. H. M., 2021)

2.7 Summary

In this chapter, a general discussion of grid-connected PV inverter systems is provided. A special attention has been paid for the role of filters to PV system. A literature review on previous research on the filter topology is also provided. Designing simulations or experimental tests is needed to validate the performance of the proposed LCL filter design. This allows for additional optimization and a deeper understanding of the actual filter performance. Lastly, a review of the factors that need to be taken into account in designing filters are also provided to be taken to the next chapter.

CHAPTER 3

METHODOLOGY

3.1 Introduction

Essentially, this chapter will be explaining about the steps used in detail throughout this study. In this study, a testing will be conducted by a simulation analysis. It is important to collect data in such a way that the results of the simulation and earlier study can be clarified and accurate. The simulation analysis was done by using a software which is a MATLAB/ Simulink. Data and results from simulation will be recorded and analyse. Throughout the chapter, the procedure for performing simulation regarding the designing LCL filter will be clarified. In this thesis, the characterised inductor is aimed to be used as a part of an LCL filter in the output of inverter. Operating at a switching frequency exceeding 20 kHz, the chosen material is the magnetic core Ferrite Toroid N87 and Ferrite Toroid T38. Ferrites demonstrate primarily hysteresis loss, and their high electrical resistivity prevents significant eddy current loss. Consequently, Ferrite stands out as the preferred material for cores operating at high frequencies (greater than 10 kHz), primarily due to its low eddy current loss.

3.2 Methodology

This thesis presents a comprehensive methodology for the design and optimization of an LCL filter for PWM PV-based inverters. The essence used in designing an LCL filter lies in achieving efficient and effective harmonic suppression while ensuring system stability and reliability. The selected approach for designing an LCL filter is based on a systematic and comprehensive methodology that takes into account of various factors and considerations which aims to get the total harmonic distortion (THD) value below 5%. The experimental method used to design the LCL filter illustrates that the design process significantly relies on practical experimentation and validation. Therefore, the steps for designing an LCL filter are shown in Figure 3.1, which is a summary of the proposed design steps of this thesis.

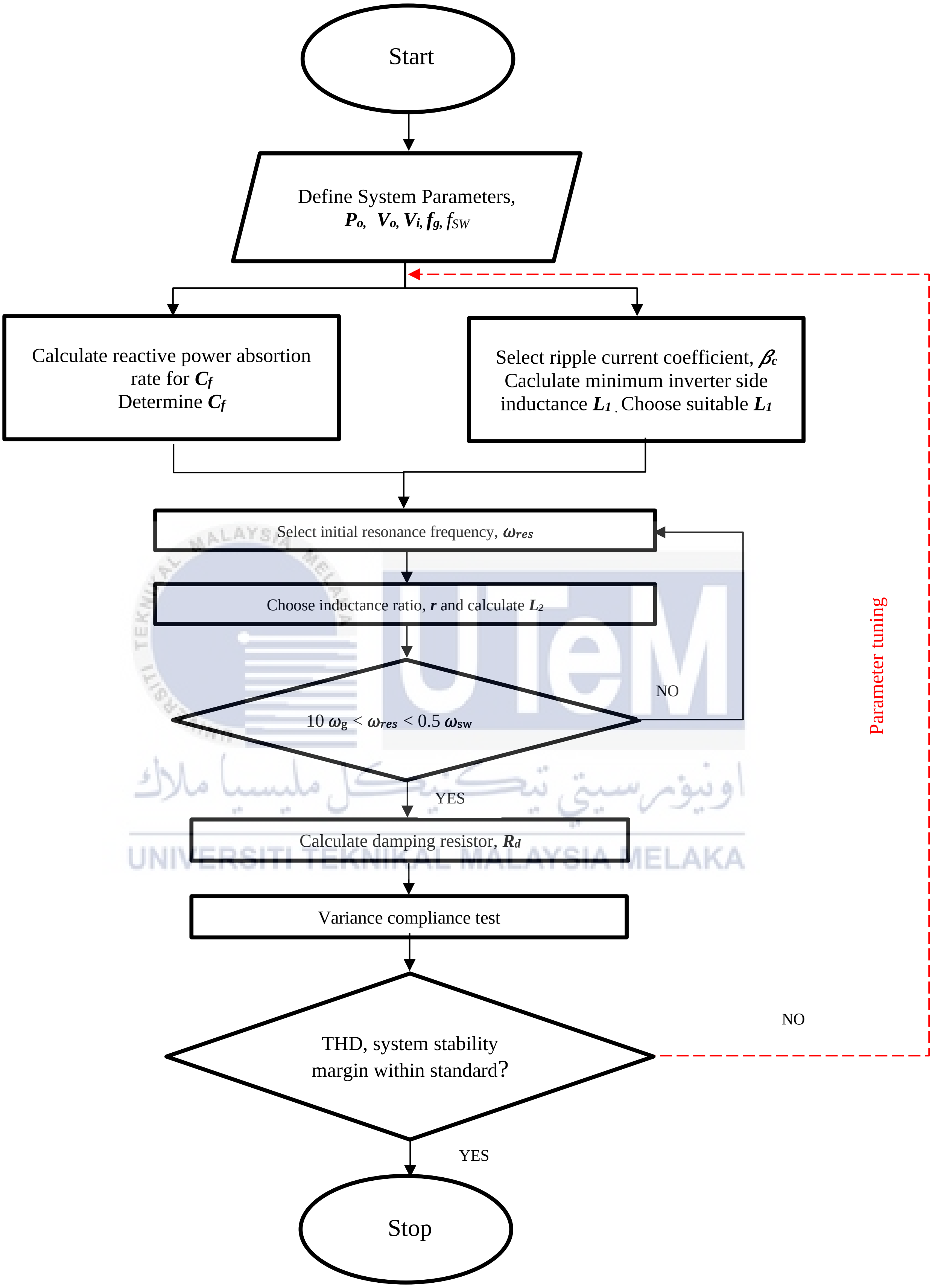

Figure 3.1 : Flowchart of LCL parameter filter design (Yaakub, M. F., Radzi, M. A. M., Azri, M., & Noh, F. H. M., 2021)

3.3 Filter Parameters

Figure 3.2 shows the basic LCL circuit while equation 2 shows the transfer function of an ideal LCL filter without damping. The equation was determined by considering the voltage at the inverter's output (V_{IN}), the grid voltage (V_{OUT}), and also the grid current (i_{L2}).

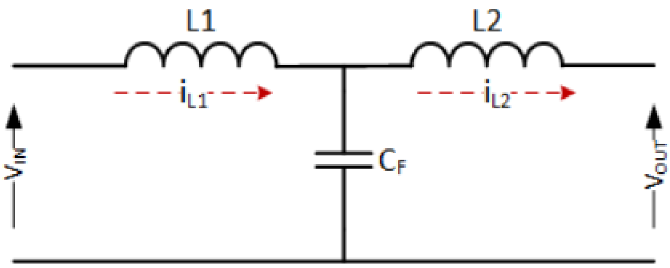

Figure 3.2 : Basic LCL filter circuit

$$G(s) = \frac{i_{L2}}{V_{IN}} = \frac{1}{L_1 L_2 C_F s^3 + (L_1 + L_2)s} \tag{3.1}$$

Figure 3.3 shows the LCL filter circuit that has added a damping resistor with a capactior. Next, by doing some simple mathematic calculation, the transfer function then becomes as shown if Equation (3.2).

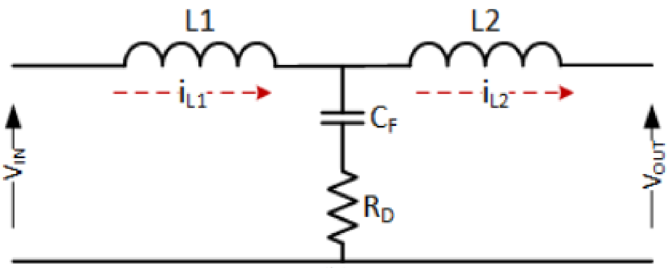

Figure 3.3 : LCL filter circuit with damping

$$\frac{i_{L2}}{V_{IN}} = \frac{C_F R_D s + 1}{L_1 L_2 C_F s^3 + C_F R_D (L_1 + L_2) s^2 + (L_1 + L_2)s} \tag{3.2}$$

Where,

R_D = Damping resistor and equivalent series resistance (ESR) of all reactive components

Following (3.1) and (3.2), the LCL filter resonance frequency can be calculated as follows:

$$\omega_{res} = \sqrt{\frac{L_T}{L_1 L_2 C_F}} \tag{3.3}$$

3.3.1 Minimum Inductance

In the LCL filter, an inductor improves current ripple control and harmonics suppression. The stiff grid system is taken into account when calculating the minimum value of inverter-side inductance, based on equation (3.4) [19].

$$L_{1min} = \frac{V_i}{8 f_{sw} I_{rpmax}} \tag{3.4}$$

Because there is a filter capacitor present in the filter network, the grid side inductor L_2 is now factorised by the inductance ratio, which is represented as r, as stated in formula (3.5)[19].

$$L_2 = rL_1 \tag{3.5}$$

3.3.2 Maximum Capacitor

Reactive power is taken into account when choosing the filter capacitor C_F. The following formula determines the maximum capacitor value for the LCL filter (3.6) [19].

$$C_{Fmax} = \frac{\alpha P_o}{\omega_o {V_o}^2} \tag{3.6}$$

Where,

αP_o = amount of reactive power that the capacitor absorbs.

V_o = rated output voltage

ω_o = grid angular frequency

Power absorption capability increases with increasing capacitance value, as shown by Equation (3.6), where absorption of reactive power is proportional to capacitance value. It's possible that if the filter's current demand goes up, the inductor's ripple current will grow and the filter's effectiveness could be affected. However, a smaller capacitance value is not preferable because a bigger inductance causes a greater voltage drop across the inductor [19].

3.3.3 Damping Resistor

Resonance reactive components arranged in parallel form the LCL filter structure as shown in formula (3.3). It is also important to understand that ω_{res} must be avoided to ensure not to overlap with harmonic sources in the circuit. The easiest method is to connect a damping resistor in series with the capacitor C_F. In general, the damping resistance should be a third of the impedance of the capacitor (3.8) [19].

$$R_d = \frac{1}{3\omega_{res} C_F} \tag{3.8}$$

3.4 LCL Filter design setup

Based on the ripple current approach, the system parameters are first determined as a part of the design process. Here, the filter is created and defined in compliance with the requirements and specifications listed in Table 3.1.

Table 3.1: System parameters specifications list.

Parameter	Symbol	Value	Unit
Rated output power	P_o	2	kW
Grid voltage	v_o	110	V
DC-Link voltage	v_i	170	V
Grid frequency	f_g	50	Hz
Switching frequency	f_{sw}	20	kHZ

For getting a wider ripple margin, the ripple coefficient at the inductor, $\boldsymbol{\beta}_c$ is set to 30% which results a minimum inductance value L_{1min} = 0.2 mH and the assume value for L_1 which is 1.0 mH is selected [19].

The maximum capacitance value is determined as C_{Fmax} = 1.64 μF using the adopting power ratio at 1.25%. By considering the production of the hardware, the assume value for the capacitors which is 1.5μF are selected [19].

The inductance ratio's value, r, need to be chosen to satisfy the resonance frequency requirement. Then, the value r = 1 is used in consideration of future hardware development from an economic standpoint [19]. It is important to comply with the resonance frequency condition 10 ω_{res} < ω_{res} < 0.5 ω_{sw}. Thus, L_2 is set to be the same as L_1, which is 1.0 mH.

Lastly, calculation of the damping resistor, Rd is equal to 5 Ω which obtain from Equation (3.8).

By considering the design setup procedure, thus the final design parameters are summarized in Table 3.2:

Table 3.2 : Final design parameters

Parameter	Symbol	Value	Unit
Capacitor	C	1.5	μF
Power ratio	α	0.0125	-
Inductor	$L_1 = L_2$	1.0	mH
Resonance frequency	ω_{res}	36514.84	Hz
Damping resistor	R_d	5.0	Ω
Angular grid frequency	ω_o	376.99	rad/s

3.5 Design simulation

Matlab/Simulink software was used to simulate the designed LCL filter. The circuit shown in Figure 3.4 below illustrates the LCL circuitry simulation together with an H-bridge voltage source inverter (VSI) in an open-loop configuration. The VSI was simulated using a unipolar SPWM switching technique using the simulation parameters indicated in Table 3.1. The goal is to make sure that the calculated values for the filter's passive parts are suitable and to study how the filter works when key component parameters change.

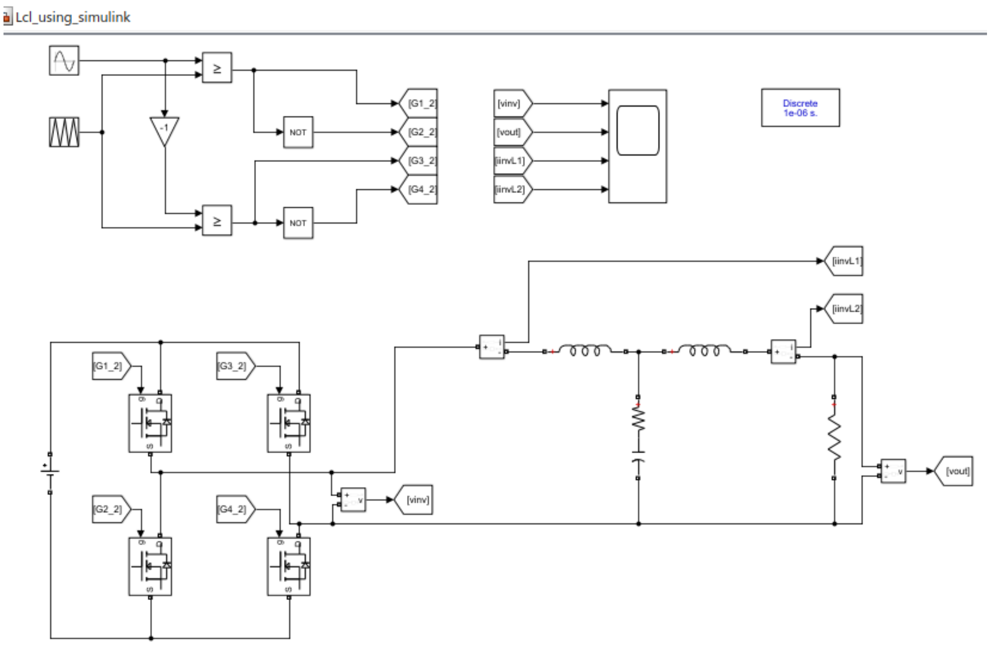

Figure 3.4 : LCL circuitry simulation together with an H-bridge voltage source inverter (VSI).

3.6 Filter circuit

After finalizing the design parameters, it is essential to draft the circuit for the filter while considering the availability of components in the market. Therefore, the following diagram shows the LCL circuit that has been designed with the component values.

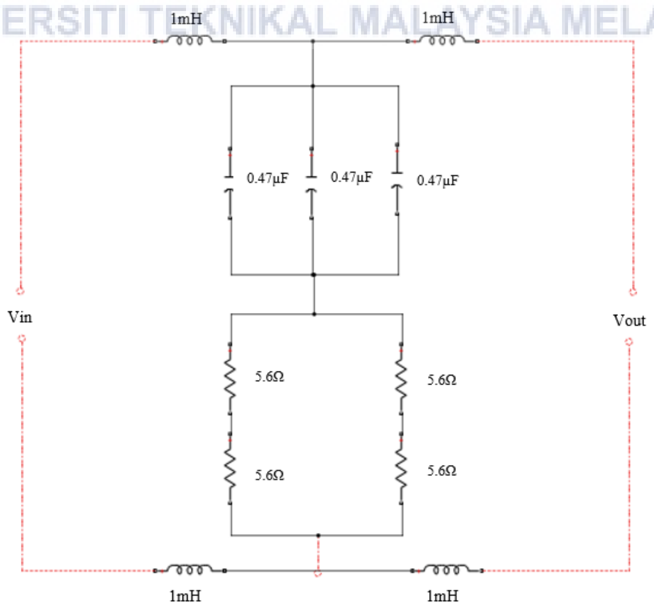

Figure 3.5 : Designed LCL circuit

3.7 Flowchart of Filter Construction

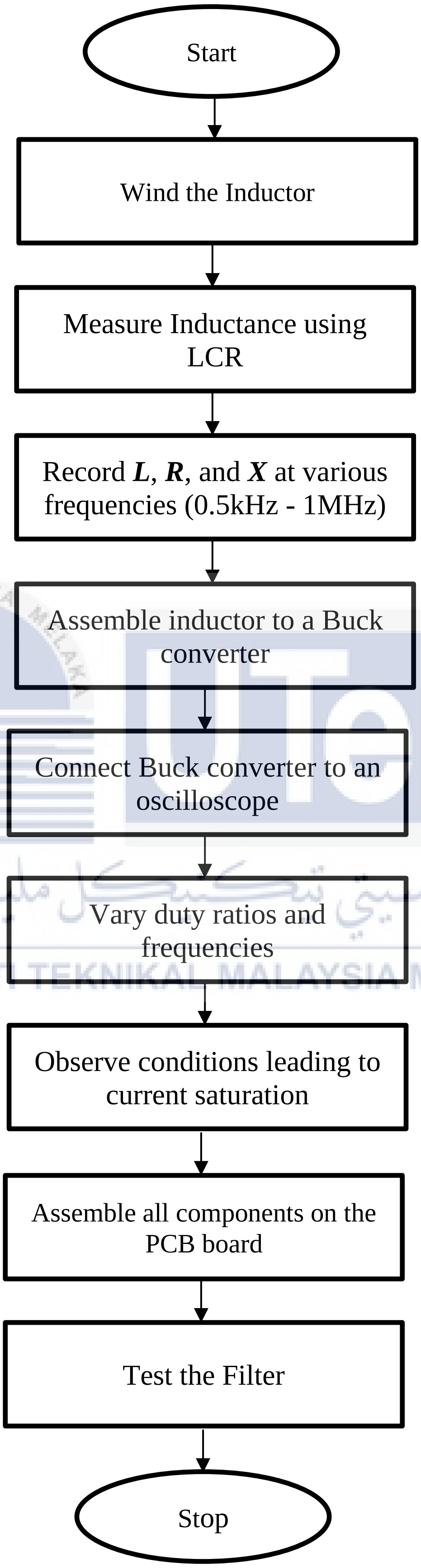

Figure 3.6 : Overview flowchart of Filter Construction

3.7.1 Inductor winding

Following Ampere's Law, we can determine the magnetic flux density within the core at any given distance r from its central axis by using formula (3.9) [27].

$$B = \frac{\mu_o \mu_r N I}{2\pi r} \tag{3.9}$$

The calculation of the magnetic flux through the cross-sectional area of the core involves dividing the area into infinitesimally thin segments with a height of ***h*** at a distance ***r*** from the axis. The sum of these segments is obtained by integrating over the radius.

$$\Phi_B = \int_S B\, ds = h \int_{r_i}^{r_o} B(r)\, dr = h \int_{r_i}^{r_o} \frac{\mu_o \mu_r N I}{2\pi r}\, dr = \frac{\mu_o \mu_r N I}{2\pi}\, h\, log_e \frac{r_o}{r_i} \tag{3.10}$$

Additionally, following the definition of inductance, we obtain the subsequent expression as formula (3.11).

$$L = \frac{N\, \Phi_B}{I} = \frac{\mu_o \mu_r N^2}{2\pi}\, h\, log_e \frac{r_o}{r_i} \tag{3.12}$$

The toroidal inductor can be parameterized as in Table 3.3.

Table 3.3: Toroidal inductor parameter

Description	Symbol	Unit
Number of turns of the coil	N	
Magnetic constant	μ_0	$T \cdot m / A$
Actual relative magnetic permeability of the core	μ_r	$T \cdot m / A$
Value of current through the coil	I	A
Core radius	r	m
Outer radius of the core	r_o	m
Inner radius of the core	r_i	m
Core height	h	m
Inductance	L	H
Magnetic flux density	B	T
Magnetic flux	Φ_B	Wb

In a simplified form, the equation appears as follows, with the core dimensions measured in millimeters and the inductance in micro-Henry.

$$L = 0.0002\ \mu_r N^2 h\ log_e \frac{OD}{ID} \tag{3.13}$$

Where ,

L = inductance of the coil

h = height of the ring

OD = outer diameter of the ring

ID = inner diameter of the ring

μ_0 = core relative magnetic permeability

3.7.2 Core type

In this project, two types of Ferrite Toroid cores have been selected for use, namely the Ferrite Toroid N87 and Ferrite Toroid T38 cores. The Figure and table below illustrates the core dimensions and characteristics [28].

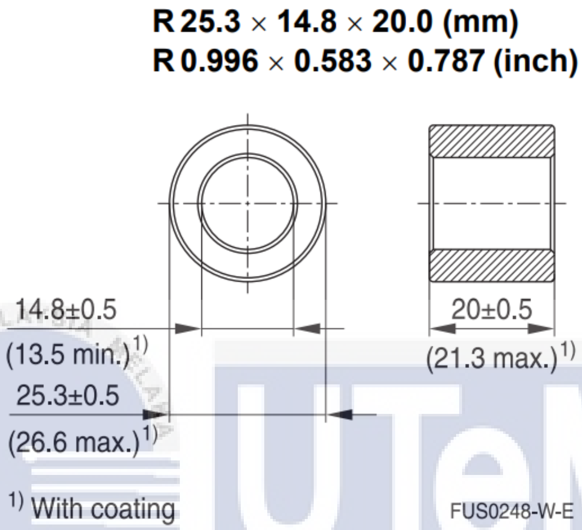

Figure 3.7 : Core dimensions

Table 3.4 : Core characteristics

Material	A_L value nH	μ_i (approx.)	Magnetic characteristics				Approx. weight g
			$\Sigma l/A$ mm^{-1}	l_e mm	A_e mm^2	V_e mm^3	
N87	4680 ±25%	2200	0.59	60.07	102.5	6157 3	33
T38	21300 ±30%	10000					

Based on the core's main specifications and utilizing formula (3.13), the number of turns required to achieve an approximate inductance value of 1.0 mH is as follows.

Table 3.5 : Number of turns for each type of core to achieve an approximate inductance value of 1.0 mH

Core type	Number of turns
N87	17
T38	8

3.7.3 Measurement of inductance

To attain the desired inductance value of 1mH with ± 10% tolerance, the utilization of a specialized instrument known as an LCR meter becomes essential as shown in Figure 3.8. The LCR meter, designed for the precise measurement of inductance, is employed in this project to accurately determine and verify the inductance parameter.

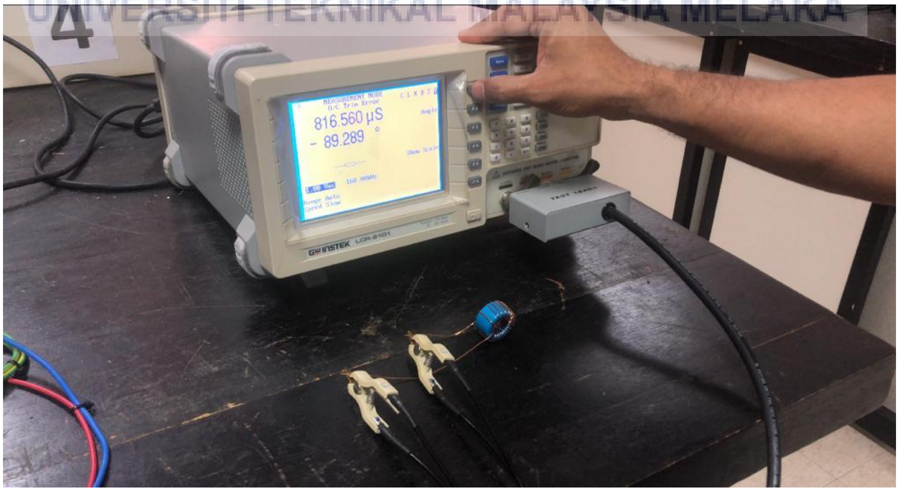

Figure 3.8 : Inductance connection to LCR meter

The series and parallel inductance together with impedance values of the toroidal inductor at different frequencies are being measured, ranging from 0.5 kHz to 1 MHz. The aim is to understand how the toroid behaves, specifically whether it acts more like an inductor or a capacitor.

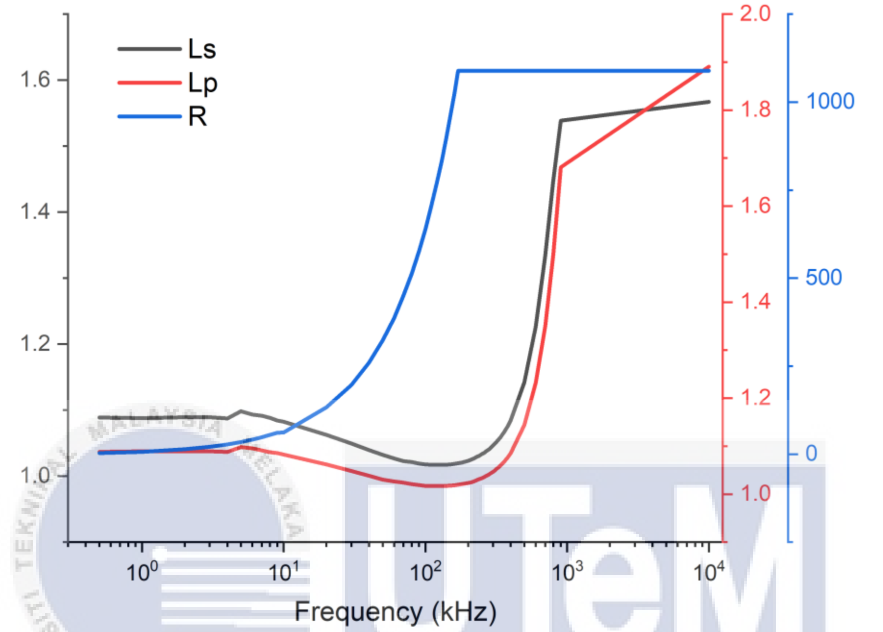

Figure 3.9 : Ferrite Toroid N87 inductor characteristic

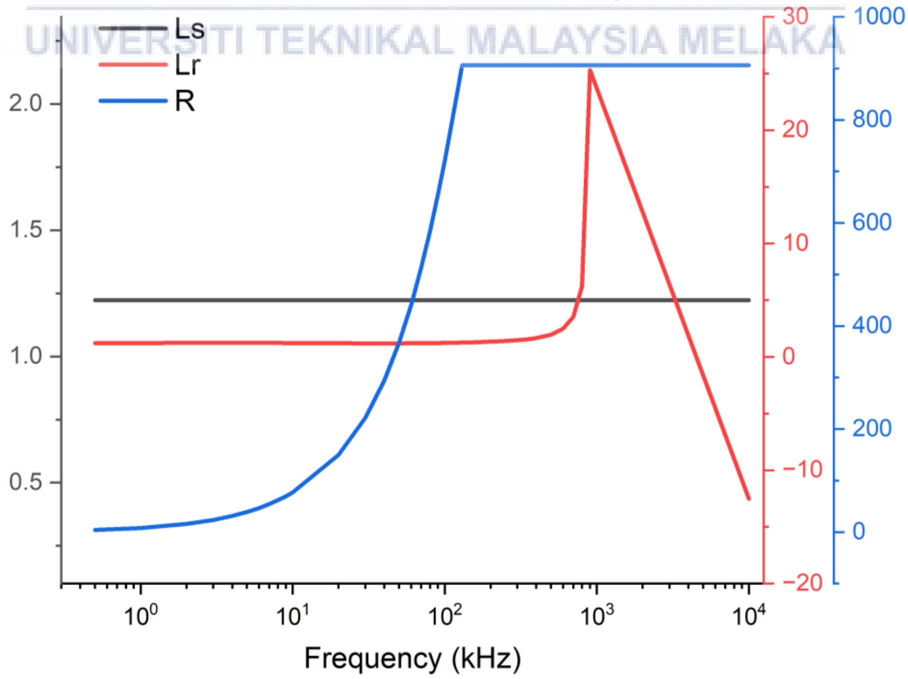

Figure 3.10 : Ferrite Toroid T38 inductor characteristic

Figure 3.9 illustrates that the inductor characteristics of the Ferrite Toroid N87 demonstrate its ability to function as an ideal inductor in both series and parallel connections. In contrast, for Ferrite Toroid T38, the characteristics change to behave like a capacitor at a frequency of 1MHz, as observed in Figure 3.10.

3.7.4 Inductor Current Profile Using Buck Converter

The wound inductor will be connected to a buck converter for precise power control, allowing adjustments to duty ratios and frequencies. Subsequently, the buck converter will be linked to an oscilloscope as shown in Figure 3.11 for real-time monitoring and analysis of the inductor's current profile under various conditions.

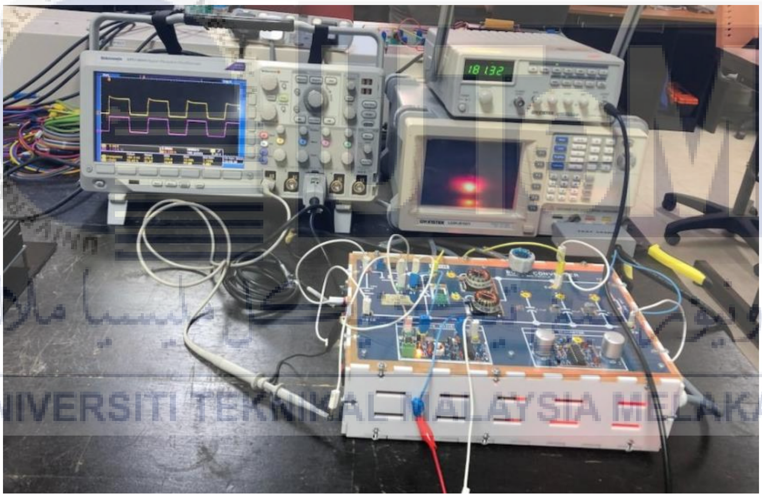

Figure 3.11 : Connection of the inductor to a buck converter and oscilloscope

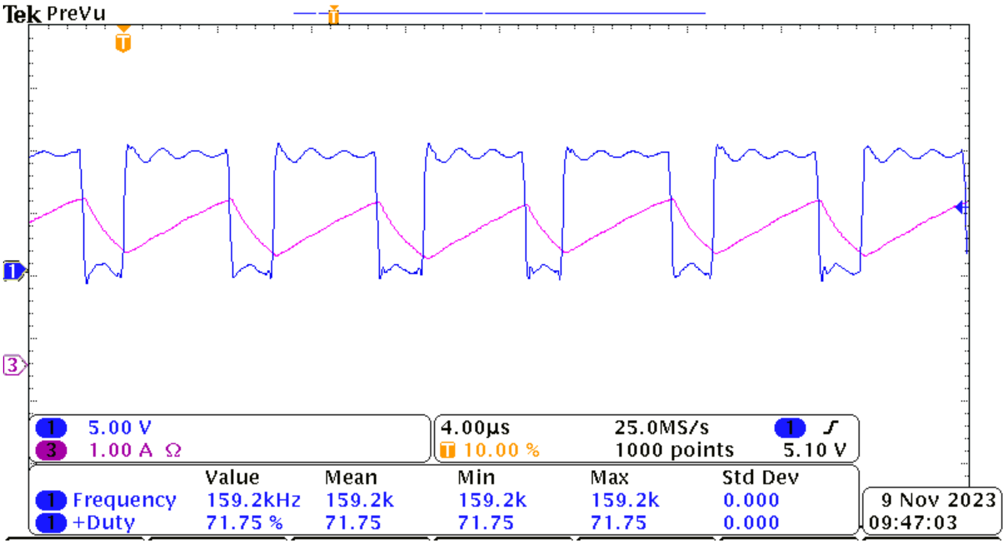

Figure 3.12: Inductor current profile

The current profile of the inductor is crucial in determining its efficiency and performance within an electrical circuit, as it influences factors such as magnetic field strength. Figure 3.12 shows that the inductor is being tested at a frequency of 160 kHz and a duty ratio of 75%. The current remains unsaturated, indicating that it can store energy, and the ripple current will not increase. This means that the efficiency will not be reduced. At this point, the inductor is behaving more like an ideal inductor and is suitable for use in this project.

3.7.5 PCB Board Assembly

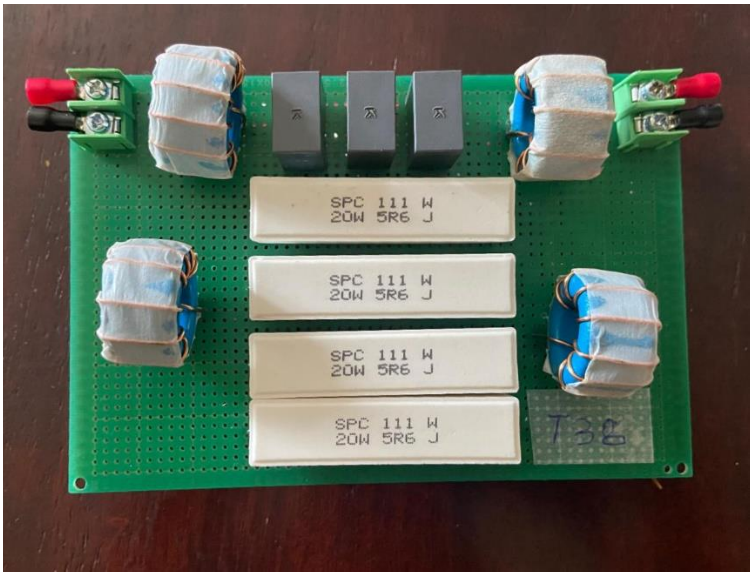

Figure 3.13: LCL filter connection

The LCL filter requires two inductors with a value of 1mH each, and two more should be placed on the negative side to handle the current. The required capacitance value is 1.41 µF, ensuring the selection of (KEMET Safety Capacitor, Metallized PP, Radial Box - 2 Pin, 0.47 µF, ± 10%, X2, Through Hole). Three of these capacitors are connected in parallel to reduce the Equivalent Series Resistance (ESR) in order to keep power dissipation low [29]. Additionally, four damping resistors (WIREWOUND RESISTOR, 5.6 OHM, 20W, 5%, AXIAL) are used. The resistors is connected in series and parallel at the same time in this circuit in order to balance or compensate for the ESR of the capacitors.

3.8 Hardware system setup

Preparing the hardware system, which involves configuring the inverter and establishing connections with the microcontroller, is a fundamental step. This process ensures that the components work well together, maintains consistency, and optimizes the experimental conditions. Ultimately, it will lead to get a more precise assessment of the performance of the hardware system, particularly when conducting tests on filters.

3.8.1 ePWM configuration using Matlab/Simulink

To achieve unipolar Pulse Width Modulation (PWM), the MATLAB configuration depicted in the figure below utilizes two Enhanced PWM (ePWM) modules. These ePWM modules are employed to control four MOSFETs, with a specified deadband unit set at 150.

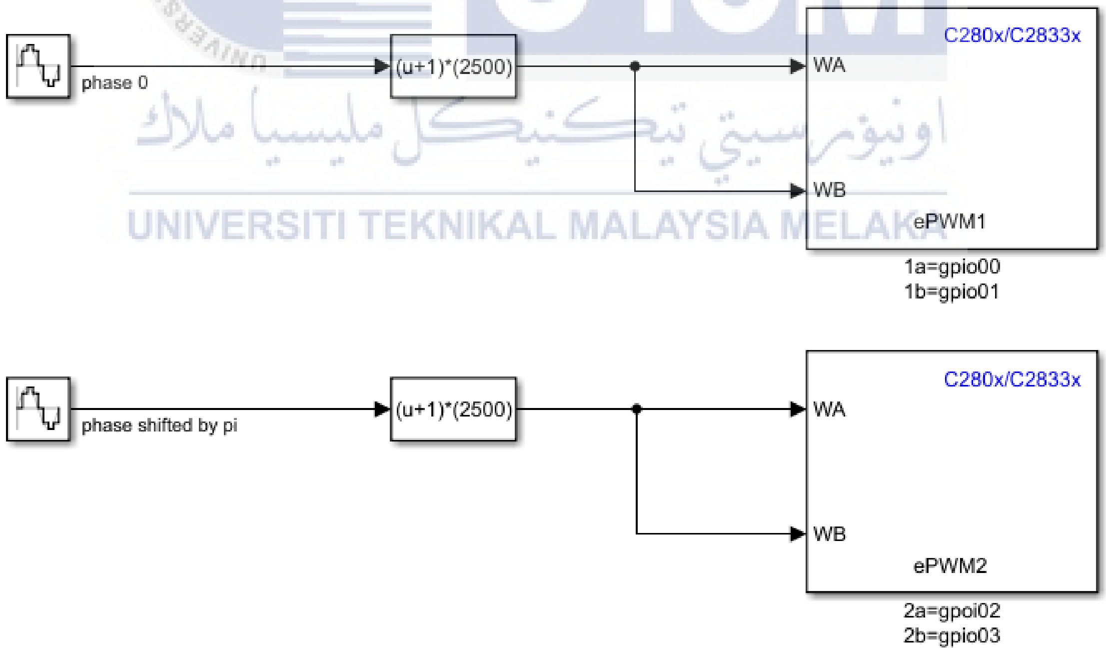

Figure 3.14: Unipolar PWM pulse controller using Matlab/Simulink

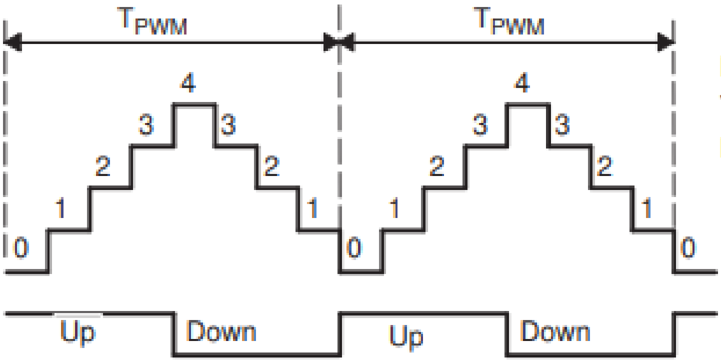

Figure 3.15: Time-Base Frequency and Period

The Down-Count Mode time-base counter is employed in this project. In this mode, the counter initiates its countdown from the specified period Time-Base Period (TBPRD) value and continues decrementing until it reaches zero [30]. Upon reaching zero, the time-base counter resets to the original period value and commences another cycle of decrementing as shown in Figure 3.15. The Time-Base Period (TBPRD) in the function block parameter is determined through the calculation by using the following equation.

$$T_{PWM} = 2 \times T_{BPRD} \times T_{TBCLK} \tag{3.13}$$

$$F_{PWM} = 1 / (T_{PWM}) \tag{3.14}$$

Where,

T_{PWM} = Time-Base Pulse Width Modulation

T_{BPRD} = Time-Base Period

T_{TBCLK} = Time-Base Clock

F_{PWM} = Frequency PWM Frequency

3.8.2 Hardware system connection

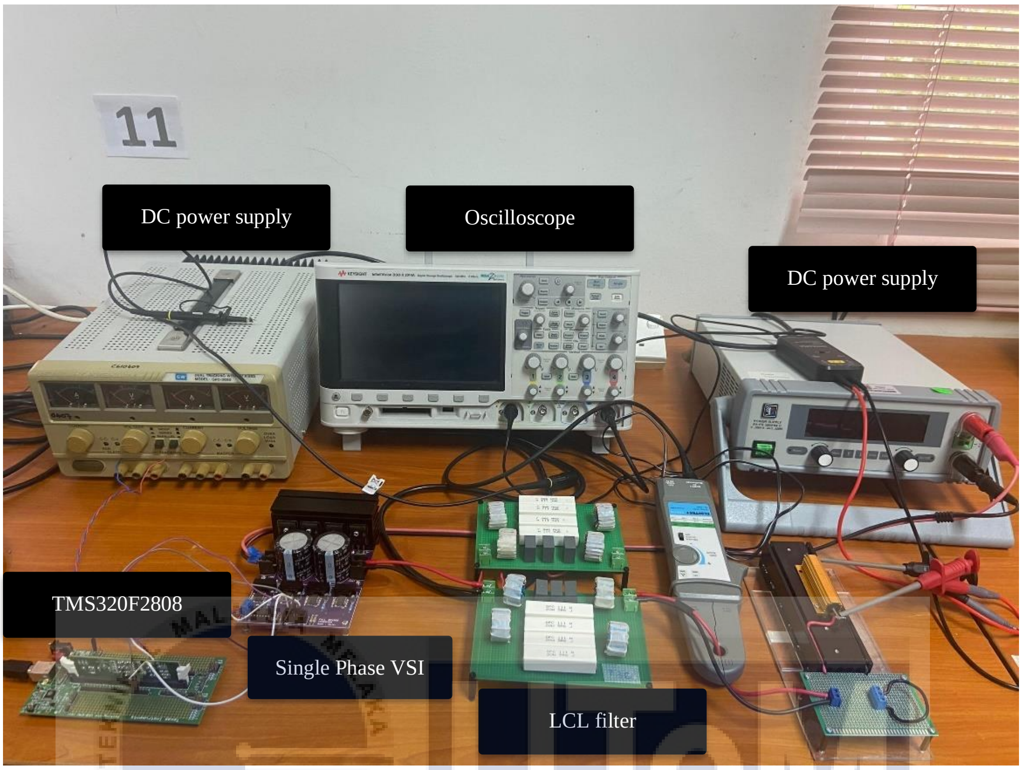

Figure 3.16: Full hardware setup

Figure 3.16 shows the complete hardware setup to test the inductor. TMS320F2808 controller is connected with a Single-phase Voltage Source Inverter (VSI) through pins GPIO00, GPIO01, GPIO02, and GPIO03, specifically designated for ePWM functionalities. The gate driver section of the inverter is powered by a 5V DC supply, while the H-Bridge section receives its supply from another DC source providing 155V. Subsequently, the inverter is connected to an LCL filter to effectively condition the output signal. Finally, the filtered signal is observed using an oscilloscope after being connected to the load. This comprehensive setup forms the basis for the investigation and analysis conducted in this project, allowing for a detailed examination of the inverter's performance and its impact on the connected load.

3.9 Summary

The chapter emphasizes the significance of different design parameters and their interrelationships in achieving an efficient LCL-filter. Two crucial factors in attaining an optimized filter are the selection of an appropriate ratio, r, between the grid-side and inverter-side inductors, and the resonance frequency. Furthermore, the chapter also suggests a design approach that must take consideration of all the variable aspects affecting an LCL-filter's performance. By defining the system parameters comprehensively, this design method considers various aspects to ensure the creation of an efficient and optimum LCL-filter.

The methodology entails a step-by-step introduction to setting up the hardware experiment, offering a systematic approach to the experimentation process. This includes configuring the inductor with two different types of permeability cores for the LCL filter to meet the objectives.

CHAPTER 4

RESULT & DISCUSSION

4.1 Introduction

In this chapter, the final design parameters obtained from the previous chapter will undergo simulation and hardware experiment. The result will be discussed to ensure that the study objective is achieved. The results of the hardware experiment will be compared between the LCL filters using N87 and T38 cores. The success will be determined based on the following outcomes:

a) Output voltage and current response

b) FFT analysis of the current

c) Comparison with IEEE recommended harmonics

4.2 Simulation output voltage and current response

In order to determine the effectiveness of the LCL filter, the pulsed of the unfiltered waveform will be compared with the filtered pulsed. The pulsed output voltage from the inverter and its filtered signal are shown in Figure 4.1, while the pulsed output current and its filtered signal are presented in Figure 4.2.

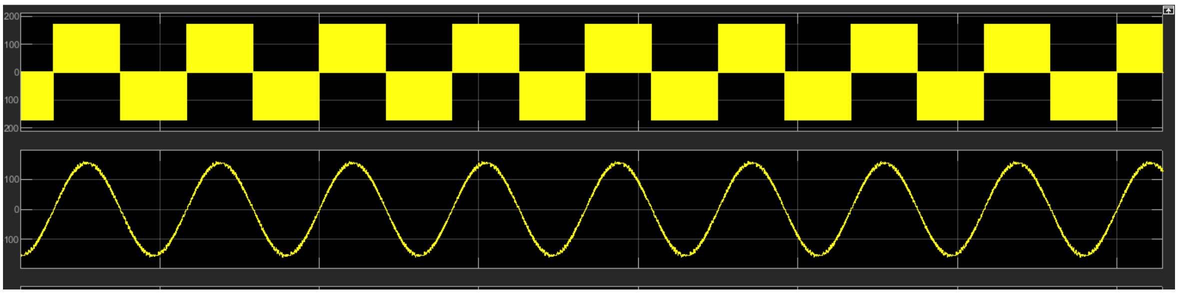

Figure 4.1 : Filtered and unfiltered output voltage

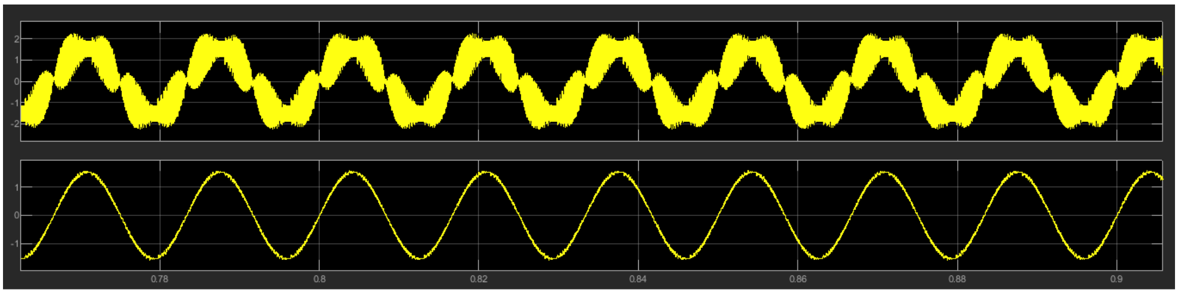

Figure 4.2 : Filtered and unfiltered output current

Observing that the ripple has decreased, it is clear that the LCL filter's output signal has improved significantly. Thus, the results above will bring benefits such as enhanced power quality and increased efficiency.

4.3 Simulation FFT Analysis of the current

In order to understand and analyze the LCL filter, unfiltered frequency content signals will be compared with the filtered frequency content signals. Figure 4.3 and 4.4 shows the Fast Fourier Transform (FFT) analysis for both filtered and unfiltered current.

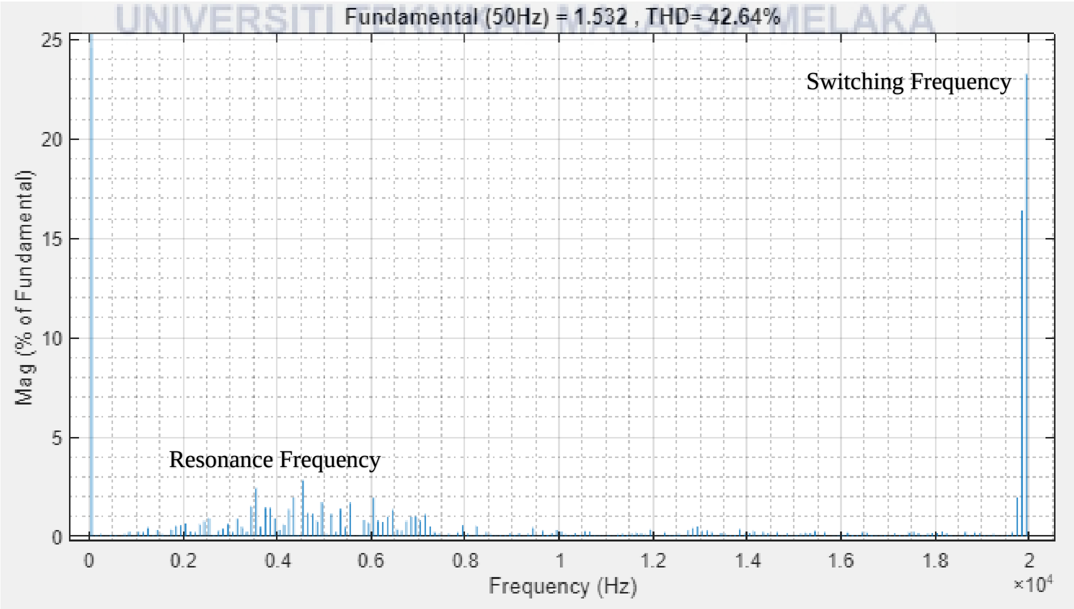

Figure 4.3: Unfiltered FFT analysis of the current.

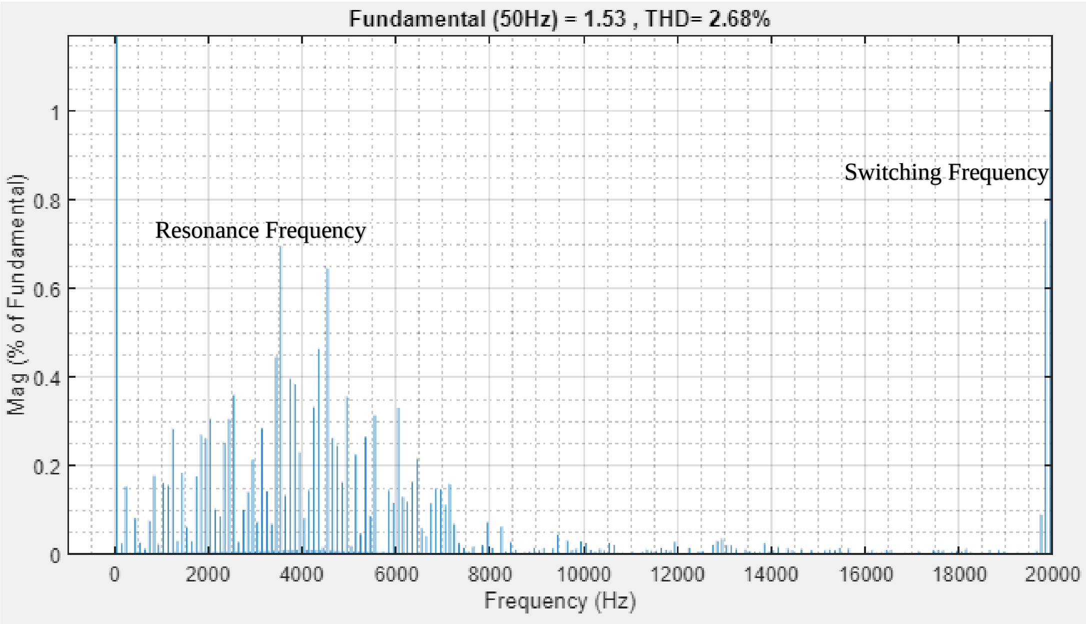

Figure 4.4: Filtered FFT analysis of the current.

The findings demonstrate that the filter effectively suppresses resonance frequency and switching frequency harmonics. The resonance frequency harmonic magnitude is attenuated from 2.9% of fundamental to only 0.7%. The same thing applies for the switching frequency harmonic, where the magnitude went from 23% of its fundamental harmonic to only 1.42% of it. These results indicate that the filter parameters are designed correctly.

4.4 Simulation comparison with IEEE recommended harmonics

The test procedure was carried out by using the current distortion limits for systems rated 120V through 69kV recommended by IEEE Std 519- 1992[7]. The analysis were performed in order to compare the behavior of the harmonics in the devices. In the next figures it can be observed the harmonic current measured and limit for each odd harmonics.

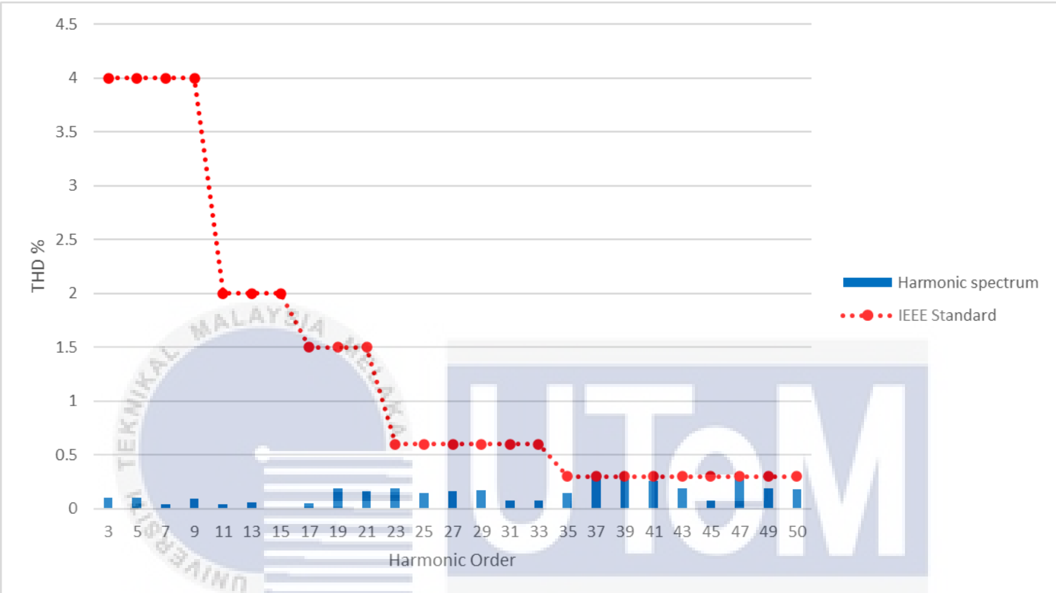

Figure 4.5: Harmonic currents measured and limits for earch odd harmonics

According to the results obtained in the Figure 4.5, each harmonics would be approved within the limits of the IEEE Std 519- 1992[7]. The magnitude of its harmonics remains significantly lower until the 33rd harmonic. Furthermore, the harmonic magnitudes of a signal become very similar after the 35th harmonic. These harmonics are mostly attenuated by the inductors in the filter structure. Thus, based on the results, it clearly demonstrates that filter systems remain stable and operate well.

4.5 Hardware output voltage and current response for N87 core type

Figures 4.6 and 4.7 displayed below illustrate the outcomes of unfiltered voltage and current signals for an LCL filter using the N87 core type. The experiment was conducted with a set frequency of 20kHz and a DC voltage of 155V. A detailed analysis of the results distinctly indicates a pronounced presence of high voltage and current ripple in the system where the magnitude for the 46V and 540mA respectively.

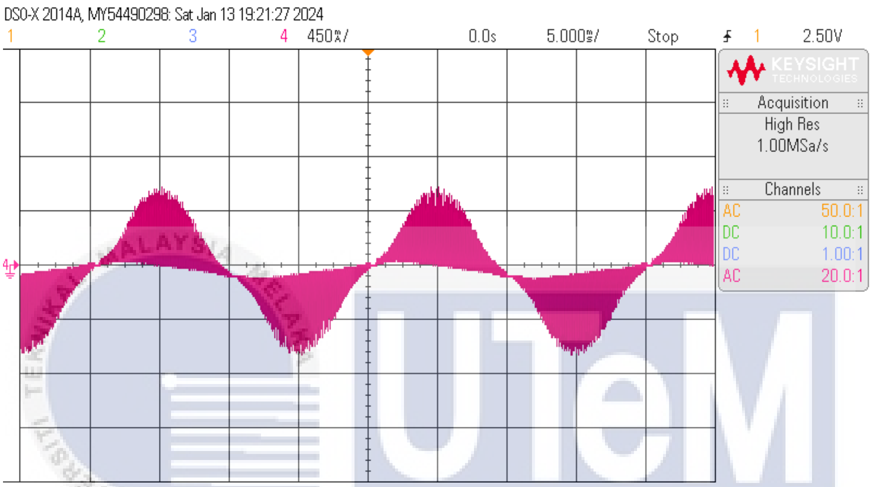

Figure 4.6: Unfiltered output current for N87

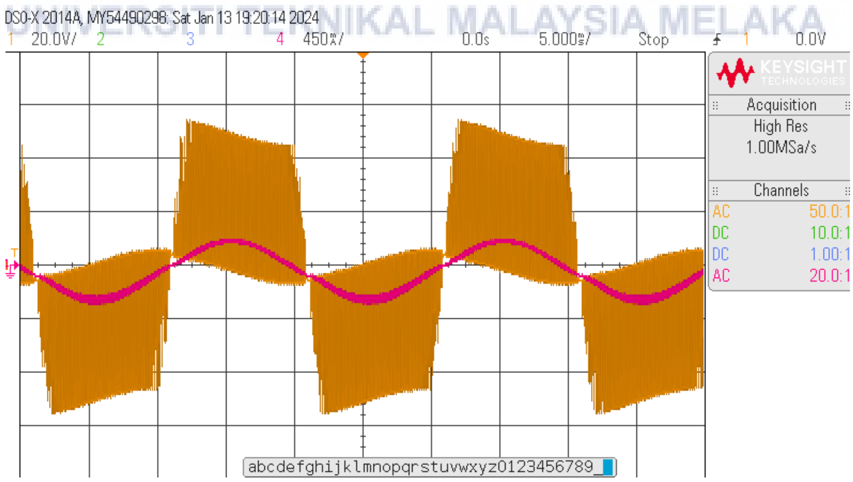

Figure 4.7: Unfiltered output voltage for N87

Figures 4.8 and 4.9 presented below show the outcomes of the filtered voltage and current signals for an LCL filter using the N87 core type. The experimental conditions were maintained at a frequency of 20kHz and a DC voltage of 155V. A comprehensive examination of the results shows a reduction in voltage and current ripple to 6V and 114mA respectively after the application of the filtering process.

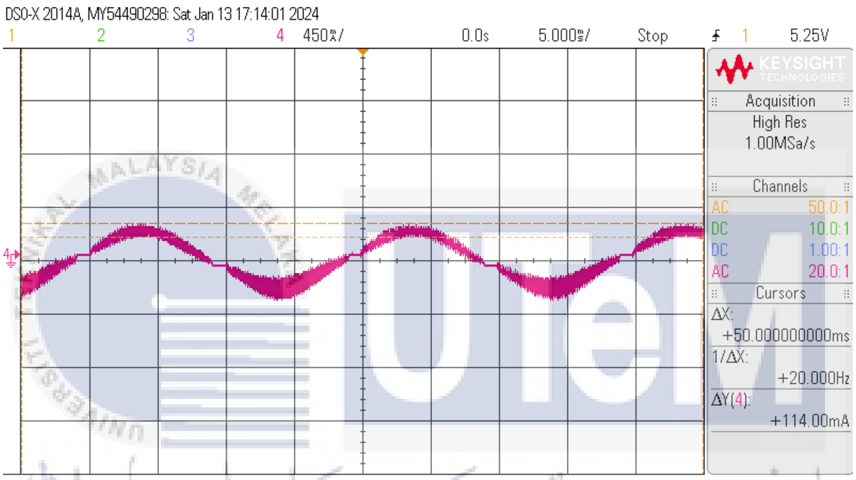

Figure 4.8: Filtered output current for N87

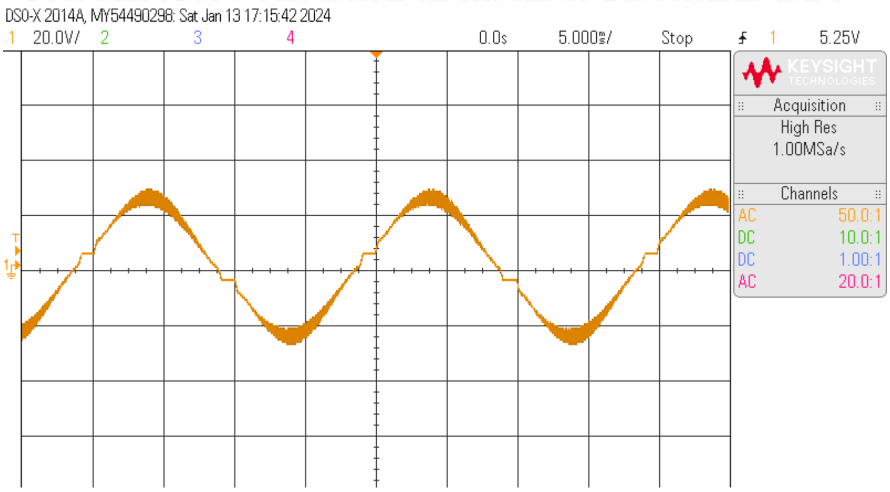

Figure 4.9: Filtered output voltage N87

4.6 Hardware FFT Analysis of the current for N87

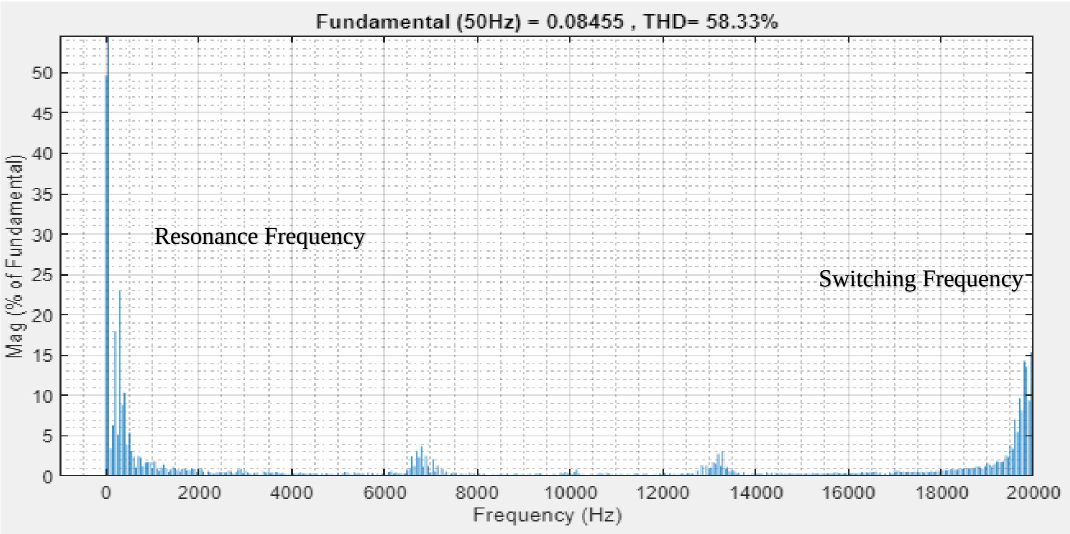

Figure 4.10: Unfiltered FFT analysis of the current for N87

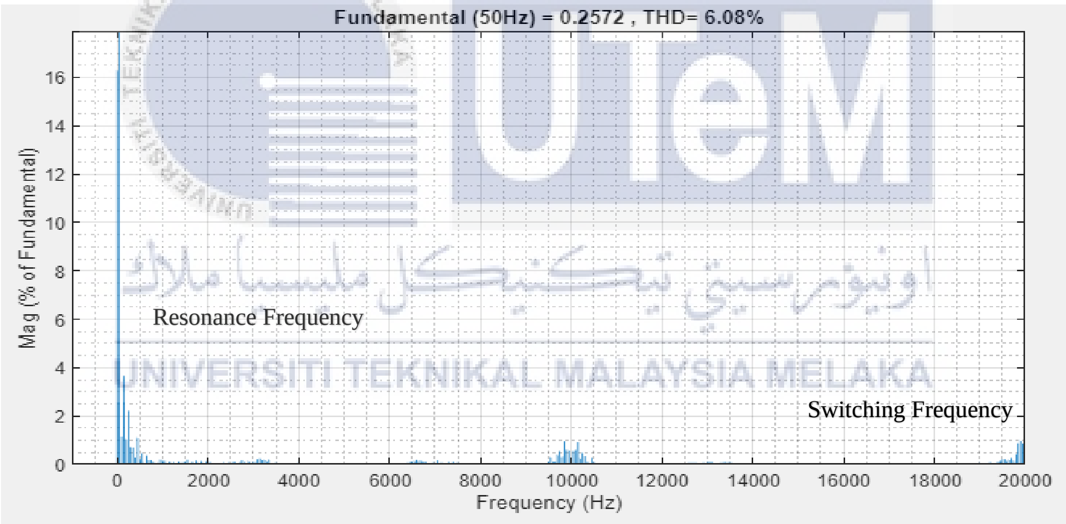

Figure 4.11: Filtered FFT analysis of the current for N87

The FFT analysis of the current in the LCL filter is conducted to evaluate the harmonic content and understand how different frequencies contribute to the overall performance of the filter. The observed trend in the FFT analysis as shown in Figure 4.10 and 4.11. The findings shows that the filter reduces the magnitude of resonance frequency and switching frequency harmonics. However, its effectiveness is limited as the Total Harmonic Distortion (THD) value does not fall below 5% as the result is 6.08%. However, the magnitude of the resonance frequency harmonic is reduced from 2.9% of the fundamental to a only 0.7%. Similarly, the switching frequency harmonic experiences a reduction, decreasing from 23% of its fundamental harmonic to only 1.42%.

4.7 Hardware comparison with IEEE recommended harmonics for N87

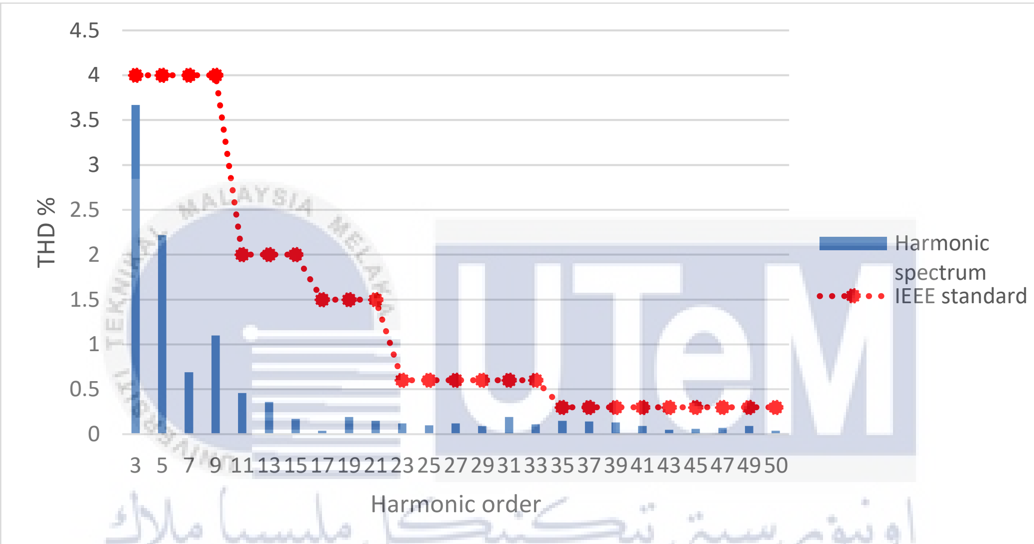

Figure 4.12: Harmonic currents measured for N87 and limits for earch odd harmonics

According to the results obtained in Figure 4.12, even though the THD value does not fall below 5%, it is important to highlight that the harmonic levels do not surpass the limit set by the IEEE Std 519-1992[7]. The magnitude of harmonics is abit high at the 3rd harmonic and remains significantly lower from the 5th up to the 13rd harmonic, and beyond the 15th harmonic, the harmonic magnitudes become very similar. Importantly, these harmonics are attenuated by the inductors in the filter structure. Therefore, based on the results, it is evident that the filter systems remain stable and operate effectively.

4.8 Hardware output voltage and current response for T38

Figures 4.13 and 4.14 presented below, shows the results of unfiltered voltage and current signals for an LCL filter utilizing the T38 core type. The experiment was conducted with a specified frequency of 20kHz and a DC link voltage of 50V. A thorough analysis of the results distinctly indicates a presence of high ripple for voltage and current in the system which is 48V and 1.08A respectively.

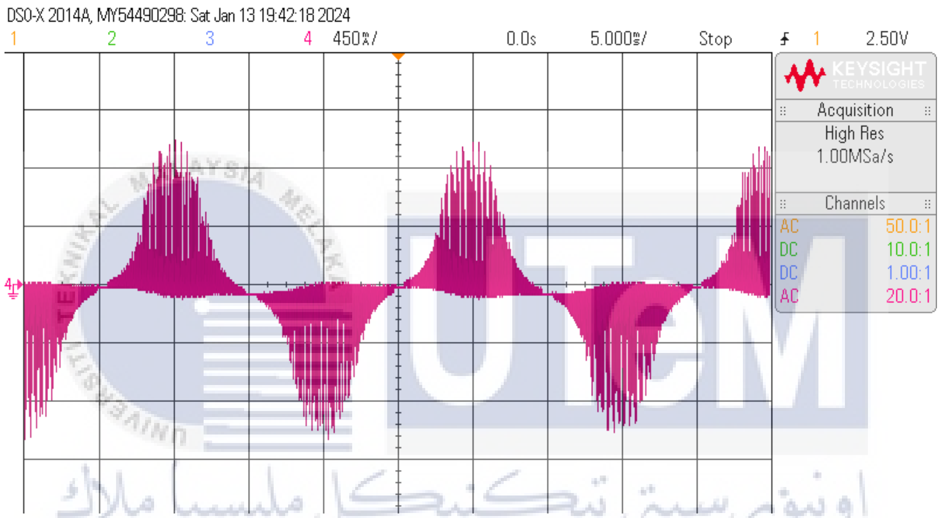

Figure 4.13: Unfiltered output current for T38

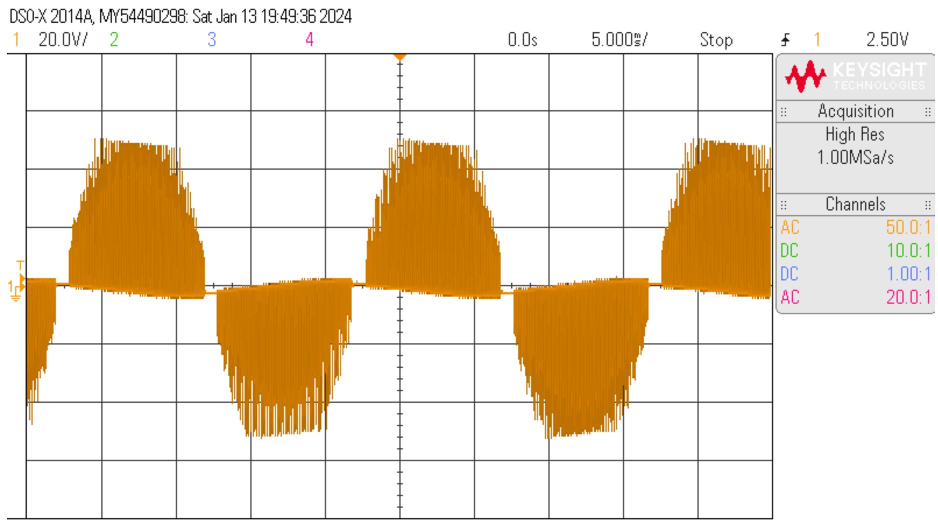

Figure 4.14: Unfiltered output voltage for T38

Figures 4.15 and 4.16 presented below show the outcomes of the filtered voltage and current signals for an LCL filter using the T38 core type. The experimental conditions were maintained at a frequency of 20kHz and a DC voltage of 50V, as the filter appears to be constrained in its ability to accommodate higher voltages starting from 80V as shown in Figure 4.17 below . A comprehensive examination of the results shows a reduction in voltage and current ripple after the application of the filtering process which is 16V and 118mA respectively.

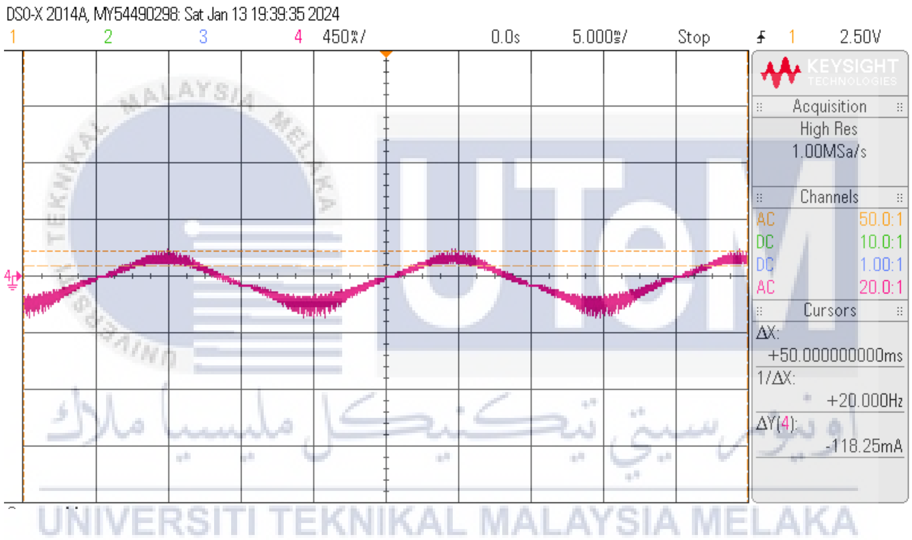

Figure 4.15: Filtered output current for T38

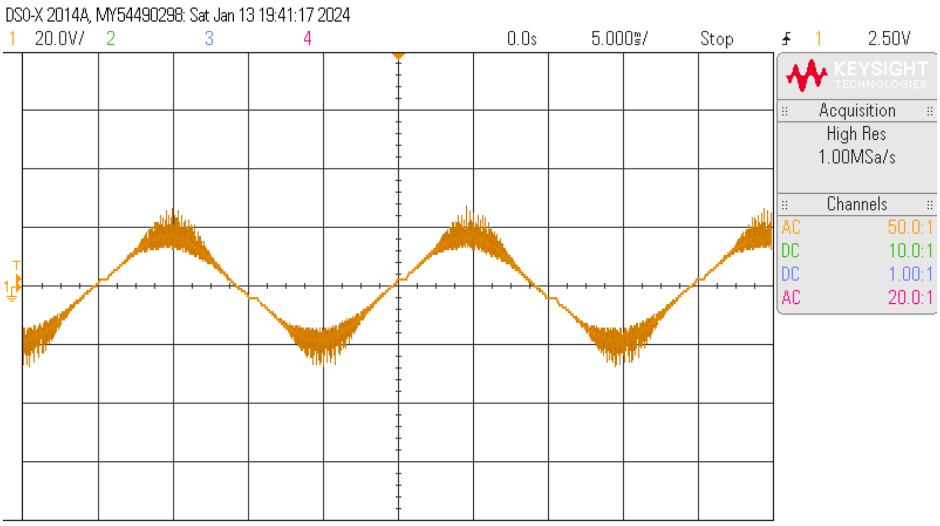

Figure 4.16: Filtered output voltage for T38 at 50V

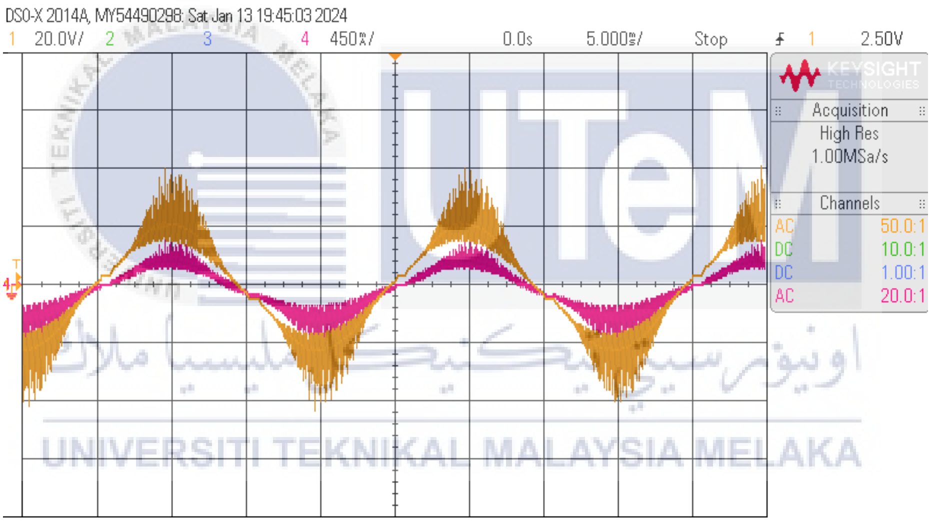

Figure 4.17: Filtered output voltage & current for T38 at 80V

4.9 Hardware FFT Analysis of the current for T38

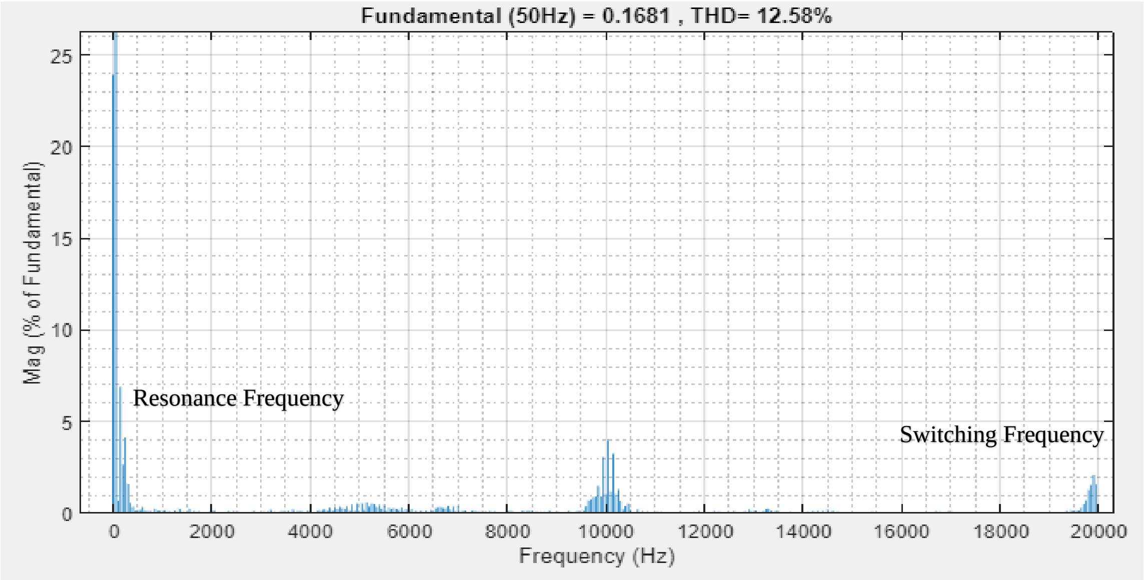

Figure 4.18: Unfiltered FFT analysis of the current for T38 at 50V

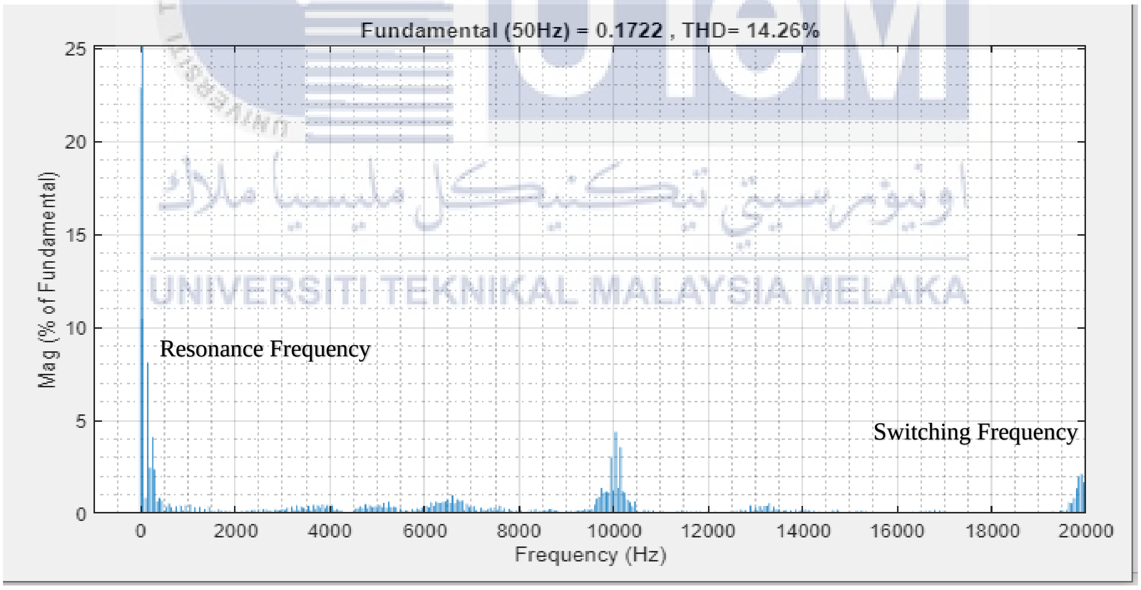

Figure 4.19: Filtered FFT analysis of the current for T38 at 80V

The observed trend in the FFT analysis as shown in Figure 4.18 and 4.19 to show the pattern in the harmonic spectrum. The findings shows that the filter reduces the magnitude of resonance frequency and switching frequency harmonics. However, its effectiveness is not good as the Total Harmonic Distortion (THD) value does not fall below 5% for both condition. From observation, the magnitude of the resonance frequency harmonic is increased from 7% (50V) of the fundamental to 8% (80V). Similarly, the switching frequency harmonic undergoes an increase, rising from 2% of its fundamental harmonic to 2.2%.

4.10 Hardware comparison with IEEE recommended harmonics for T38

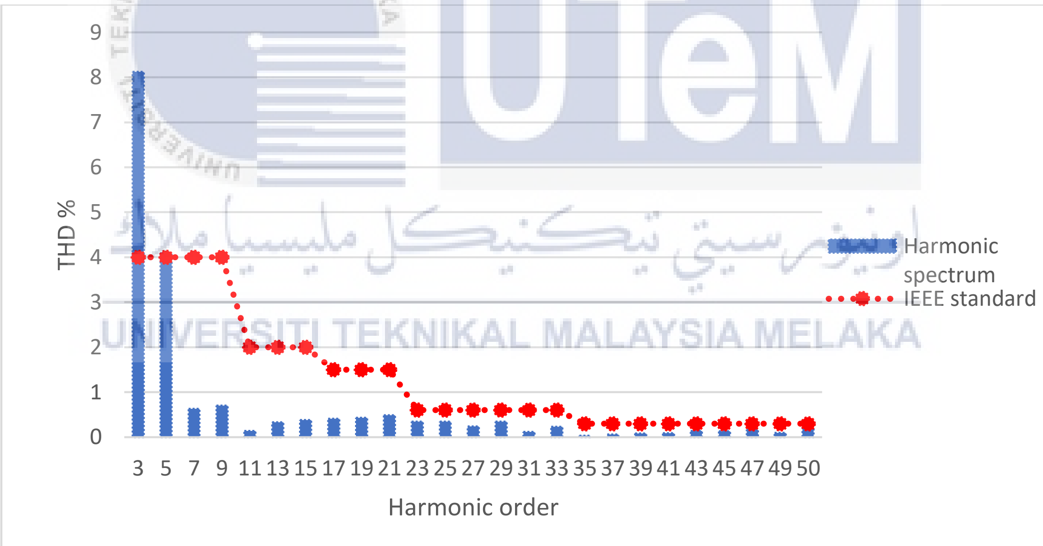

Figure 4.20: Harmonic currents measured for N87 at 50V and limits for earch odd harmonics

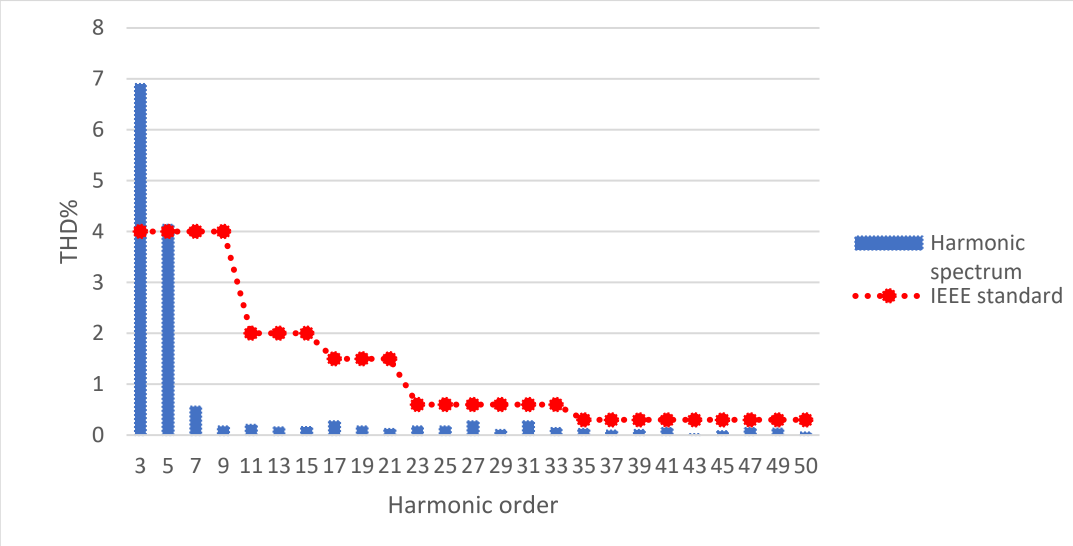

Figure 4.21: Harmonic currents measured for N87 at 50V and limits for earch odd harmonics

Based on the results shown in Figures 4.20 and 4.21, it's clear that the Total Harmonic Distortion (THD) is exceed above 5%. Notably, some harmonic levels go beyond the limits set by the IEEE Std 519-1992[7]. Specifically, at 50V, the 3rd and 5th harmonics are at 6.9 and 4.09, respectively. When we increase the voltage to 80V, the THD goes up, and the 3rd and 5th harmonics also increase to 8.12 and 4.09, respectively. This highlights the need to address harmonic levels to meet established standards.

4.11 Discussion

Table 4.1: Performance of two filter core types

Filter core type	DC Voltage, V	Unfilered		Filtered		Percentage of reduction (%)		THD, %
		Current, mA	Voltage, V	Current, mA	Voltage,V	Current	Voltage	
N87	155	540	46	114	6	78.89	86.96	6.08
T38	50	1080	48	118	16	89.07	66.67	12.58
	80	1080	48	270	28	75.00	71.43	14.26

The table presents comparative data on the performance of two filter core types, N87 and T38, in terms of reducing DC voltage and total harmonic distortion (THD) under various conditions. The N87 core type demonstrates a notable reduction in both voltage and current, with percentage reductions of 78.89% and 86.96%, respectively. In contrast, the T38 core type exhibits varying performance based on different initial DC voltages, achieving reductions in voltage ranging from 75.00% to 89.07% and in current from 66.67% to 71.43%. However, the THD values for T38 are comparatively higher (ranging from 12.58% to 14.26%) than the N87's 6.08%, indicating potentially greater distortion in the filtered signal for T38. The choice between N87 and T38 would likely depend on specific application requirements, considering factors such as the desired level of voltage/current reduction and acceptable THD levels. Further experimentation and analysis are warranted to comprehensively understand the performance characteristics of these filter core types in diverse operating conditions.

4.12 Summary

This chapter presented the importance of the outcomes we need to analyse to design filters for PWM-based PV inverters. The simulation results support the theoretical results in terms of current suppression, reduction in signal frequency content, and compliance with IEEE Standard 519-1992 [7]. The suggested design steps resulted in a stable filter configuration that satisfies the required specifications, with acceptable amounts of total harmonic distortion (THD). Thus, the experimental results confirm the theoretical achievements.Additionally, the filter was constructed using parameters employed in the simulation. The results indicated that utilizing N87 core type yielded superior filtering outcomes compared to T38 core type, highlighting that lower permeability cores which is N87 are less susceptible to saturation effects, especially in applications with high AC currents.

CHAPTER 5

CONCLUSIONS & RECOMMENDATION

5.1 Conclusions

In summary, this thesis has suggested the design of the LCL filter for PWM based PV inverter. Many previous researches have been referred in order to achieve the objective of this study. The process of designing this filter has been explained step by step based on the requirements and specifications of the filter design. The examples of requirements that need to be considered to find the parameter values to design this filter are inductance ratio, damping resistor and resonance frequency. On the other hand, the simulation was carried out using Matlab/Simulink software to prove that the theoretical value is valid through experiment. As a result, the observation from the simulation is valid by complying with the standard proposed by IEEE 519-1992, where the THD produced by the filter is not more than 5%. In conclusion, the results obtained from the simulation have proven the success of the theoretical value.

After constructing the filter with parameters used in the simulation, this thesis aimed to achieve its second objective by testing two filters with different core permeabilities. The results revealed that lower permeability cores, specifically the N87 core type, are less susceptible to saturation effects, a critical factor in applications with high AC currents, making them superior to the T38 core type. Comparing the outcomes, N87 demonstrated lower ripple and better support for greater voltage, contributing to the efficiency of the PV system.

5.2 Recommendation

As for recommendation, it is advisable to explore the use of another core type, T65, within the project to assess its impact on signal behavior. Additionally, to ensure proper connections and minimize parasitic elements in the filter circuit, employ precision soldering methods. Consider using a PCB board to further enhance stability, reduce impedance, and overall improve the performance of the filter. The use of oscilloscope with Total Harmonic Distortion (THD) readings also will make easier to ensure that the filter meets the standard set by the IEEE 519-1992, providing a comprehensive evaluation of different core types and their suitability for optimal performance in the photovoltaic system.

REFERENCES

[1] Zhang, N., Tang, H., & Yao, C. (2014, June 24). A Systematic Method for Designing a PR Controller and Active Damping of the LCL Filter for Single-Phase Grid-Connected PV Inverters. Energies, 7(6), 3934–3954

[2] Tsai, C., & Chen, S. (2012). PV Power-Generation System with a Phase-Shift PWM Technique for High Step-Up Voltage Applications. International Journal of Photoenergy, 2012, 1–11

[3] Hamza O Khalfalla, (2019), A Study of Adaptive proportional resonant controller for singlephase grid-connected PV inverter based on grid impedance estimation technique

[4] R. Kadri, J. Gaubert, and G. Champenois, "An Improved Maximum Power Point Tracking for Photovoltaic Grid-Connected Inverter Based on VoltageOriented Control," IEEE Transactions on Industrial Electronics, vol. 58, pp. 66-75, 2011.

[5] G. M. Dousoky, E. M. Ahmed and M. Shoyama, "MPPT schemes for single-stage three-phase grid-connected photovoltaic voltage-source inverters," 2013 IEEE International Conference on Industrial Technology (ICIT), Cape Town, South Africa, 2013, pp. 600-605, doi: 10.1109/ICIT.2013.6505739.

[6] Borni, A., Abdelkrim, T., Bouarroudj, N., Bouchakour, A., Zaghba, L., Lakhdari, A., & Zarour, L. (2017, July). Optimized MPPT Controllers Using GA for Grid Connected Photovoltaic Systems, Comparative study. Energy Procedia, 119, 278–296.

[7] IEEE Recommended Practices and Requirements for Harmonic Control in Electric Power Systems, IEEE Std. 519-1992, 1992

[8] Namboodiri, A.V., & Wani, H.S. (2014). Unipolar and Bipolar PWM Inverter.

[9] Liqaa Alhafadhi, (2016), A Study of Total Harmonics Distortion Reduction Using Adaptive, Weiner, and Kalman Filters.

[10] M. Safwan b. M. Masarik, (2017), A Study of Design of Lowpass Filter with Low Total Harmonic Distortion.

[11] Almaita EK. Adaptive Radial Basis Function Neural Networks-Based Real Time Harmonics Estimation and PWM Control for Active Power Filters [dissertation]. Western Michigan University; 2012.

[12] Alhafadhi L, Teh J. Advances in reduction of total harmonic distortion in solar photovoltaic systems: A literature review. Int J Energy Res. 2019;1–16.

[13] Liqaa Alhafadhi, (2016), A Study of Total Harmonics Distortion Reduction Using Adaptive, Weiner, and Kalman Filters.

[14] Deepika Kumari. (2014), A Study of Optimal LCL Filter Design For Gridinterfaced Distridbuted Power Generation System.

[15] Villanueva, I., Vazquez, N., Vaquero, J. M. M., Hernández, C. G., López, H. S., & Osorio, R. (2020). L vs. LCL Filter for Photovoltaic Grid-Connected Inverter: A Reliability Study. International Journal of Photoenergy, 2020, 1–10.

[16] Parikshith B.C, (2009), A study of Integrated Approach to Filter Design for Grid Connected Power Converters.

[17] Kean, Y. W., Yong, P., Ramasamy, A. K., & Ramachandaramurthy, V. K. (2015). Comparison of the effect of filter designs on the total harmonic distortion in three-phase stand-alone photovoltaic systems. ARPN Journal of Engineering and Applied Sciences, 10(21), 9919–9925.

[18] Cha H., Vu T. K. (2009). Study and Design of L-C-L Filter for Single-Phase Grid-Connected PV Inverter.

[19] Yaakub, M. F., Radzi, M. A. M., Asri, M., Shafie, S., Azis, N., & Noh, F. H. M. (2021). LCL filter design based on ripple current minimization approach for grid-connected inverter application. 2021 IEEE Industrial Electronics and Applications Conference (IEACon).

[20] P. Channegowda and V. John, “Filter optimization for grid interactive voltage source inverters,” IEEE Trans. Ind. Electron., vol. 57, no. 12, pp. 4106-4114, Dec. 2010.

[21] S. Jayalath and M. Hanif, "Generalized LCL-Filter Design Algorithm for Grid-Connected Voltage-Source Inverter," in IEEE Transactions on Industrial Electronics, vol. 64, no. 3, pp. 1905-1915, March 2017, doi: 10.1109/TIE.2016.2619660.

[22] Y. Tang, W. Yao, P. C. Loh and F. Blaabjerg, "Design of LCL-filters with LCL resonance frequencies beyond the Nyquist frequency for grid-connected inverters," 2015 IEEE Energy Conversion Congress and Exposition (ECCE), Montreal, QC, Canada, 2015, pp. 5137-5144, doi: 10.1109/ECCE.2015.7310384.

[23] Attia, H., Che, H. S., Freddy, S., & Elkhateb, A. (2019). Design of LLCL Filter for Single Phase Inverter with Confined Band Variable Switching Frequency (CB-VSF) PWM. Journal of Power Electronics, 19(1), 44–57.

[24] Yaakub, M. F., Radzi, M. A. M., Azri, M., & Noh, F. H. M. (2021). LCL filter design for grid-connected single-phase flyback microinverter: a step by step guide. International Journal of Power Electronics and Drive Systems (IJPEDS), 12(3), 1632.

[25]] R. Pena-Alzola, M. Liserre, F. Blaabjerg, M. Ordonez, and Y. Yang, (2014) “LCLfilter design for robust active damping in grid-connected converters,” IEEE Trans. Ind. Informat., vol. 10, no. 4, pp. 2192–2203, Nov

[26] Liserre, M., Blaabjerg, F., & Hansen, S. (2005). Design and Control of an LCL-FilterBased Three-Phase Active Rectifier. IEEE Transactions on Industry Applications, 41(5), 1281–1291.

[27] Arfken, G. (2012, December 2). University Physics. Academic Press.

[28] TDK Electronics AG, Ferrites and accessories Toroids ring cores, (May 2023)

[29] S. Prasanth et al., "Condition Monitoring of Electrolytic Capacitor based on ESR Estimation and Thermal Impedance model using Improved Power Loss Computation," 2018 International Power Electronics Conference (IPEC-Niigata 2018 -ECCE Asia), Niigata, Japan, 2018, pp. 416-421, doi: 10.23919/IPEC.2018.8507747.

[30] Texas Instruments. (2023). TMS320F28004x Real-Time Microcontrollers Technical Reference Manual (Literature Number: SPRUI33G).